Spatiotemporal variations of shallow very low frequency earthquake activity southeast off the Kii Peninsula, along the Nankai Trough, Japan

Shunsuke Takemura[1,1,1], Kazushige Obara[2,2,2], Katsuhiko Shiomi[3,3,3], and Satoru Baba[1,1,1]

[1]Earthquake Research Institute, the University of Tokyo
[2]Earthquake Research Institute, The University of Tokyo
[3]National Research Institute for Earth Science and Disaster Resilience

November 30, 2022

Abstract

Cross-correlation analysis was applied to long-term onshore broadband records from April 2004 to March 2021 to detect and relocate shallow very low frequency earthquakes (VLFEs) southeast off the Kii Peninsula, along the Nankai Trough, Japan. We then determined the moment rate functions of detected shallow VLFEs using the Monte Carlo-based simulated annealing method. According to this new comprehensive catalog, shallow VLFEs are widespread beneath the accretionary prism toe, but shallow VLFEs with large cumulative moments are localized around the western edge of the paleo-Zenisu ridge, which is subducted beneath southeast off the Kii Peninsula. This finding indicates that the subducted ridge causes heterogeneous structures and stress conditions that promote shallow slow earthquakes. The relocated shallow VLFE epicenters illustrated three major episodes characterized by a similar activity area and five minor episodes characterized by different areas. The three major episodes exhibited slow frontal migration with different initiation locations, directions, and speeds, as well as several rapid reverse migrations. Episodes of minor activity were distributed in different locations within part of the area of major activity. According to our results and the geometry of the plate boundary, we conclude that the subducted ridge also plays an important role in the activity area of shallow VLFE episodes. Different patterns of shallow VLFE migration could reflect temporal changes in the pore-fluid distribution or stress conditions of the plate boundary.

Spatiotemporal variations of shallow very low frequency earthquake activity southeast off the Kii Peninsula, along the Nankai Trough, Japan

Shunsuke TAKEMURA[1], Kazushige OBARA[1], Katsuhiko SHIOMI[2], Satoru BABA[1]

[1]Earthquake Research Institute, the University of Tokyo, 1-1-1 Yayoi, Bunkyo-ku, Tokyo, 113-0032, Japan.

[2]National Research Institute for Earth Science and Disaster Resilience, 3-1 Tennodai, Tsukuba, Ibaraki, 305-0006, Japan.

Corresponding author: Shunsuke TAKEMURA (shunsuke@eri.u-tokyo.ac.jp)

Key Points:

- We estimated the locations and moment rate functions of shallow very low frequency earthquakes that occurred near the Nankai Trough
- Large cumulative moments of shallow very low frequency earthquakes were concentrated in the region with the subducted oceanic ridge
- The migration of shallow very low frequency earthquakes exhibits various patterns in terms of initiation, migration direction, and area

Abstract

Cross-correlation analysis was applied to long-term onshore broadband records from April 2004 to March 2021 to detect and relocate shallow very low frequency earthquakes (VLFEs) southeast off the Kii Peninsula, along the Nankai Trough, Japan. We then determined the moment rate functions of detected shallow VLFEs using the Monte Carlo-based simulated annealing method. According to this new comprehensive catalog, shallow VLFEs are widespread beneath the accretionary prism toe, but shallow VLFEs with large cumulative moments are localized around the western edge of the paleo-Zenisu ridge, which is subducted beneath southeast off the Kii Peninsula. Our results from long-term shallow VLFE catalog are well consistent with previous studies in this region, suggesting that heterogeneous structures and stress conditions due to the subducted paleo-Zenisu ridge promote the occurrence of shallow slow earthquakes. The relocated shallow VLFE epicenters illustrated three major episodes characterized by a similar activity area and five minor episodes characterized by different areas. The three major episodes exhibited slow frontal migration with different initiation locations, directions, and speeds, as well as several rapid reverse migrations. Episodes of minor activity were distributed in different locations within part of the area of major activity. Different patterns of shallow VLFE migration could reflect temporal changes in the pore-fluid distribution or stress conditions of the plate boundary.

Plain Language Summary

Our knowledge of the physical characteristics of shallow slow earthquakes, which may provide frictional properties on plate boundaries and preparation processes of large interplate earthquakes, is still limited. Thus, we comprehensively analyzed shallow very low frequency earthquakes (VLFEs) southeast off the Kii Peninsula, in the Nankai subduction zone, where large tsunamigenic earthquakes have repeatedly occurred with intervals of approximately 100–200 years. We found that shallow VLFEs occurred around the western edge of the subducted oceanic ridge. We considered that this ridge causes complex stress and subsurface structures around the plate boundary and consequently promotes slow earthquake activity.

1 Introduction

In various subduction zones, megathrust earthquakes have repeatedly occurred at intervals of several hundred years as a result of accumulated shear stress caused by plate subduction. The stress accumulation and release processes on the plate boundary are important for the earthquake cycle and source physics. Slow earthquakes can release part of accumulated stress on the plate boundary. Slow earthquakes occur as slips on the plate boundary; however, their rupture durations are significantly longer than those of regular earthquakes with a similar magnitude (summarized in Ide et al., 2007; Obara & Kato, 2016). Slow and regular interplate earthquakes are separately distributed on the plate boundary (e.g., Baba et al., 2021; Dixon et al., 2014; Nishikawa et al., 2019; Plata-Martinez et al., 2021; Takemura, Okuwaki, et al., 2020; Vaca et al., 2018), reflecting the heterogeneous distribution of effective strength and stress conditions. Thus, studies of the source processes of both slow and regular interplate earthquakes are important for understanding and monitoring stress accumulation on the plate boundary.

Slow earthquakes occur on various timescales. Tectonic tremors and very low frequency earthquakes (VLFEs) are recorded at seismic stations in frequency ranges of 2–8 Hz and 0.02–0.05 Hz, respectively. The geodetic observations detect slow slip events (SSEs), with durations ranging from several days to several years. Spatiotemporal correlations among these various earthquake phenomena have also been reported, which are referred to as episodic tremor and slip (ETS; Hirose & Obara, 2006; Ito et al., 2007; Rogers & Dragert, 2003). Dense onshore seismic and geodetic observations have allowed us to analyze the source characteristics of deep slow earthquakes that occur around the deeper extensions of megathrust seismogenic zones. In Nankai and Cascadia subduction zones, various physical characteristics of deep slow earthquake sources have been reported (e.g., Bostock et al., 2015; Ide et al., 2008; Michel et al., 2019; Supino et al., 2020). Shallow slow earthquakes occur at shallower extensions of megathrust zones and are often considered possible triggers of megathrust earthquakes (e.g., Kato et al., 2012, 2016; Vaca et al., 2018; Voss et al., 2018). However, owing to the lack of long-term offshore observations and strong offshore heterogeneities around source regions, our knowledge of the characteristics of shallow slow earthquake sources is still limited. As such, a stable and accurate analysis of long-term observation records is required to discuss the characteristics of shallow slow earthquakes, which may provide key information on the shear strength and structural conditions on shallow plate boundaries.

In this study, we investigate the source and migration characteristics of shallow VLFEs that occurred southeast off the Kii Peninsula, Japan (Figure 1) within 15–35 km from the Nankai Trough (deformation front). Along the Nankai Trough, megathrust earthquakes have repeatedly occurred at intervals of 100–200 years (e.g., Ando, 1975), and various shallow slow earthquake phenomena have been detected (e.g., Annoura et al., 2017; Araki et al., 2017; Kaneko et al., 2018; Obara & Ito, 2005). Takemura, Noda, et al. (2019) revealed that shallow VLFEs tend to migrate in the regions surrounding the shear stress accumulation peaks on the Philippine Sea Plate boundary. However, they only detected and relocated shallow VLFEs during episodes that started from September 2004, March 2009, and April 2016. Moreover, they only discussed epicenter locations and migration characteristics of shallow VLFEs. Thus, in this study, we comprehensively detect and relocate all shallow VLFEs from April 2004 to March 2021 (a period of 17 years). Then, we estimate the moment rate functions of detected shallow VLFEs using Green's functions of the local three-dimensional (3D) model in order to determine their source characteristics. Detailed tectonic environments, such as velocity structures and slip-deficit rate estimations, have been studied southeast off the Kii Peninsula (e.g., Agata, 2020; Akuhara et al., 2020; Noda et al., 2018; Park et al., 2002, 2004; Tonegawa et al., 2021). Thus, a high-resolution moment-rate-function catalog of long-term shallow VLFE activity allows us to discuss characteristics of the spatial pattern of slips due to shallow slow earthquakes southeast off the Kii Peninsula. We also discuss the migration of shallow VLFEs.

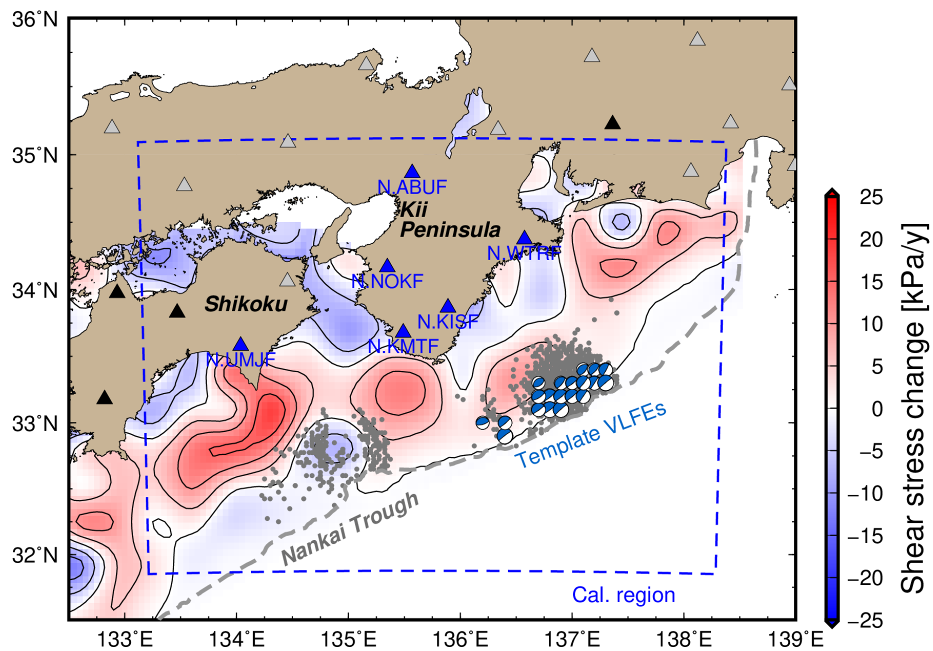

Figure 1. Map of the Nankai subduction zone. Gray circles are the epicenters of shallow VLFEs detected in our previous study (Takemura, Noda, et al., 2019). Blue focal spheres are the template shallow VLFEs, which are well-constrained centroid moment tensor solutions derived from Takemura, Matsuzawa, et al. (2019). Triangles are the F-net stations. Stations with black and blue filled triangles were used in the template matching and relocation analysis. Stations represented by gray triangles were not used in the analysis. Estimates of moment rate functions for the detected VLFEs were derived from data at the blue filled triangles. Blue dashed rectangle represents the horizontal calculation region for Green's functions. Background color represents the shear stress change rate on the plate boundary caused by the subduction of the Philippine Sea Plate (Noda et al., 2018).

2 Data and Methods

To detect shallow VLFEs southeast off the Kii Peninsula in the Nankai subduction zone, we used three-component continuous velocity records at full-range seismogram network (F-net) broadband stations from April 2004 to March 2021. F-net is operated by the National Research Institute for Earth Science and Disaster Resilience (NIED; Aoi et al., 2020). Although data from the Dense Oceanfloor Network system for Earthquakes and Tsunamis (DONET) has been available since August 2011, F-net covers a longer observation period. In particular, two large shallow VLFE episodes occurred in September 2004 and March 2009, prior to the deployment of DONET. Using the method of Takemura, Noda, et al. (2019), we performed template matching and relocation analysis of shallow VLFEs southeast off the Kii Peninsula. For the detection and moment rate function estimation, we selected the frequency band of 0.02–0.05 Hz to enhance small shallow VLFE signals and avoid the period bands of microseisms at onshore seismic stations (e.g., Nishida, 2017).

We then calculated the cross-correlation coefficients (CCs) between the filtered template and observed seismograms every 1 s. The blue focal spheres in Figure 1 show the template events of shallow VLFEs, whose template waveforms can be downloaded from the supporting information of Takemura, Noda, et al. (2019). Assuming 3.8 km/s as the propagation velocity of surface wave, the CCs at the stations were back-propagated to possible shallow VLFE epicenters, which were uniformly distributed at an interval of 0.025°. After averaging the CCs at the stations for each time and grid, we detected the events with average CCs ≥ 0.45 as shallow VLFE candidates. To avoid regular earthquakes and duplicate detections, we removed the local regular earthquakes listed in the unified hypocenter catalog of the Japan Meteorological Agency (JMA) and selected a shallow VLFE candidate with the maximum CC every 60 s. Because of the station distribution, our method constrained the shallow VLFE epicenters along the strike direction (Figure S1). Figures 1bd of Takemura, Noda, et al. (2019) show comparisons of epicenters between our previous catalog and Nakano et al. (2018). The relocated epicenters of Takemura, Noda, et al. (2019) were in good agreements with Nakano et al. (2018), especially in the along-strike direction. In Figure S1, relatively high (> 0.5) CCs appeared within 30-50 km from the optimal epicenter. Due to the wavelengths of surface waves used in this study, each template can catch shallow VLFE candidates occurring within 30-50 km from a template epicenter. After our detection process and automatic removal of local regular earthquakes listed in the JMA catalog, we obtained 2,776 candidates of shallow VLFEs in this region.

After detection and relocation, we estimated the moment rate functions of the detected shallow VLFEs using the Monte Carlo-based simulated annealing technique. Surface wave propagation from shallow VLFEs to F-net stations is significantly affected by the 3D heterogeneous structures of the accretionary prism, the Philippine Sea Plate, and seawater (e.g., Nakamura et al., 2015). Thus, we prepared Green's functions in the local 3D model via reciprocal calculations using an open-source seismic wave propagation code (OpenSWPC; Maeda et al., 2017). The simulation model covered an area of 360×480×80 km^3 (blue dashed rectangle in Figure 1), discretized by grid intervals of 0.2 km in the horizontal direction and 0.1 km in the vertical direction. The assumed 3D velocity model was constructed by combining the Japan Integrated Velocity Structure Model (JIVSM; Koketsu et al., 2012) and 1D velocity models beneath DONET stations (https://doi.org/10.5281/zenodo.4158946; Tonegawa et al., 2017). The detailed model construction process was described previously by Takemura, Yabe, et al. (2020). The possible source grids were similar to those in the relocation analysis. Each reciprocal calculation for preparing 200-s Green's functions required 727 GB of computer memory and 2 h of computation time using 48-node hybrid (OpenMP/MPI) parallel computation on the Fujitsu PRIMERGY CX600M1/CX1640M1 (Oakforest-PACS) at the Information Technology Center, the University of Tokyo.

The moment rate function estimation procedure is as follows. The epicenter and depth were fixed at the location after VLFE relocation and the depth of the upper surface of the JIVSM Philippine Sea Plate. Because shallow VLFEs are characterized by low-angle thrust faulting (e.g., Sugioka et al., 2012; Takemura, Matsuzawa, et al., 2019), focal mechanisms were also fixed as low-angle thrust faulting constructed by the plate geometry of JIVSM and convergence directions of NUVEL-1A (DeMets et al., 2010). The JIVSM was constructed to evaluate the hazard of long-period ground motion caused by anticipated large earthquakes in Japan (https://www.jishin.go.jp/evaluation/seismic_hazard_map/lpshm/12_choshuki/). More detailed plate models southeast off the Kii Peninsula exist (e.g., Park et al., 2004; Yamamoto et al., 2017), but our analysis based on very low frequency (0.02-0.05 Hz) surface waves is expected to be insensitive to fine-scale plate geometry (e.g., Figure 10 of Takemura, Okuwaki, et al., 2020).

In this study, the moment rate function was constructed using a series of Küpper wavelets with a duration of 6 s. The synthetic velocity waveform $v_{ij}(t)$ from the j-th source grid to the i-th station can be written as follows:

$$v_{ij}(t) = A_0 \sum_{k=0}^{N_P-1} w_k^2 G_{ij}(t - k\Delta t),$$

where G_{ij} is the Green's function of the j-th source with a unit 6-s Küpper wavelet, w_k^2 is the weight of the k-th Küpper wavelet, and Δt is the offset of each pulse (3 s). Non-negative conditions w_k^2 were imposed in our estimation. The parameter A_0 is the optimal relative amplitude estimated by fitting observed waveforms to synthetic waveforms based on variance reduction (Yabe et al., 2021). Using the observed waveform and amplitude-adjusted model seismogram v^{syn}, the objective function used in this analysis was

$$E = \sum_i \sum_l \left| v_{ij}^{obs}(t_l + \tau) - v_{ij}^{syn}(t_l) \right|$$

where τ is the delay time and the length of the time window is 200 s (t_l = 0–200 s). The parameters w_k^2 and τ were estimated via the Monte Carlo-based simulated annealing procedure. At each iteration step, Δw = 0.02 and $\Delta\tau$ = 0.5 s were perturbed for the source weights (w_k) and delay time (τ), respectively. According to shallow VLFE duration measurements derived from offshore broadband analysis (Sugioka et al., 2012), the number of source weight parameters was 40; thus, the maximum duration of the modeled moment rate function was 123 s. We note that our method cannot sufficiently catch source moment release at lapse times after 120 s because used onshore F-net stations are located at 100-260 km from source grids. The parameters of the initial temperature ($T_0 = 3E_0$) and cooling rate ($\gamma = 0.996$) in the simulated annealing were similar to those in Tocheport et al., 2007. We initially assumed $w_k^2 = 1$, which could not reproduce the observed seismograms (Figure 2b). The annealing schedule at the k-th iteration was given by $T_k = \gamma^k T_0$. Thus, in the case of γ very close to 1, the convergence toward the global minimum can be slow. The perturbation at the k-th iteration with ΔE_k ($=E_k-E_{k-1}$) < 0 was fully accepted. We also accepted the perturbation with $\Delta E_k \geq 0$ and the probability of $P = \exp(-\Delta E_k/T_k)$ equal to less than α, which is a random number between 0 and 1 at each iteration. This procedure allows to escape from a local minimum.

An example of the moment rate function estimation is shown in Figure 2. The gray line in Figure 2a represents the original estimate of the moment rate function via the simulated annealing method. Because our estimations were conducted using a frequency band of 0.02–0.05 Hz, longer duration small tail at times after about 30 s (i.e., the later part of the gray line in Figure 2a) may not contribute to the reproducibility of the observed seismograms for frequencies of 0.02–0.05 Hz. In addition, for cases with a low signal-to-noise ratio, our method might model reverberations of later weak surface waves within oceanic sediments and noise signals as a seismic moment release from the source. Therefore, to avoid misestimation of moment rate functions after the simulated annealing procedure, especially due to noise signals, we calculated the variance reductions (VRs) between observed and synthetic seismograms, which were constructed using N Küpper pulses. We adopted up to the N-th ($N = 1$–40) parameters, which achieved 90 % of the maximum VR (VR_m) for the simulated annealing result. The gray and blue lines in Figure 2a show the results of the original simulated annealing and optimal solutions, respectively. The synthetic seismograms obtained using the optimal solution reproduced the observed seismograms (Figure 2c). The synthetic seismograms from the original full simulated annealing result and the optimal solution were not much different (Figure S2), indicating longer duration tail of the estimated moment rate function did not contribute to the reproducibility of observed seismograms for frequencies of 0.02-0.05 Hz. Although we adopted the solutions with 90 % of the VR_m in later discussions (Figures 3–7), we also tested other VR thresholds for 85 % and 95 % of the VR_m (Figures S3–S8).

After obtaining the optimal solution, we calculated the VR values between the observed and optimal syntenic seismograms. These VR values represent the goodness-of-fit factors for the optimal solutions. For shallow VLFEs with lower VRs (< 30 %), the signals at onshore F-net stations can be weak compared to the noise signals; consequently, their durations might be misestimated due to low signal-to-noise ratio conditions. Therefore, in subsequent discussions of shallow VLFE activities, we discarded the results with VRs < 30 %.

Finally, we visually checked all shallow VLFE candidates. We removed surface wave signals from earthquakes at regional-to-teleseismic distances. In our study, we detected shallow VLFE candidates every 60 s. Some shallow VLFEs can be characterized by long (> 60 s) duration moment rate function. Thus, we also removed duplicate counts of longer-duration shallow VLFEs, which occurred at very close locations and timing.

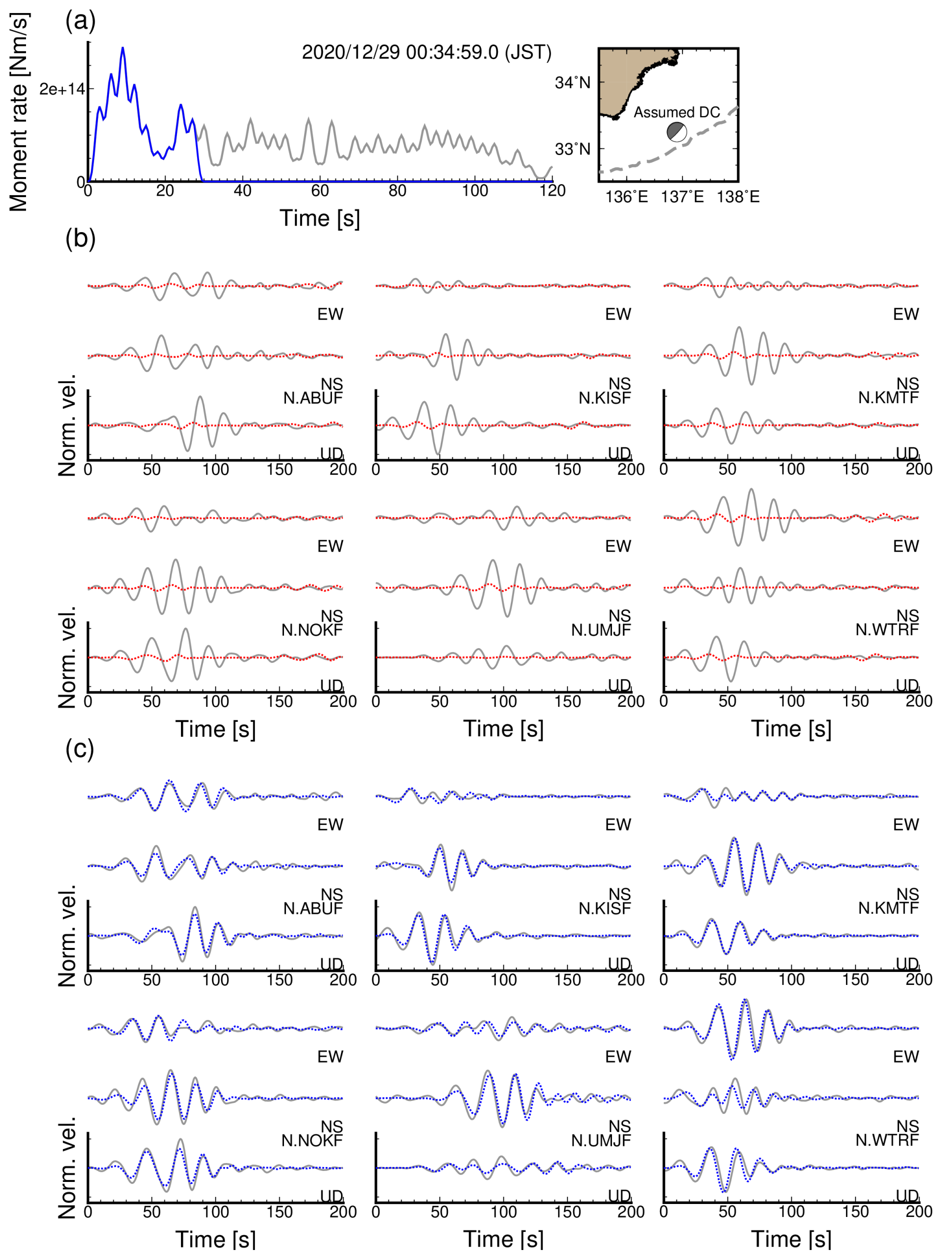

Figure 2. An example of moment rate function estimation for a shallow VLFE that occurred at 00:34:59.0 on 29 December 2020 (JST). (a) Estimated moment rate function, (b) comparisons between observed and initial synthetic waveforms, and (c) comparisons between observed and optimal waveforms. The assumed double-couple (DC) focal mechanism in the map was constructed using the plate geometry of JIVSM (Koketsu et al., 2012) and the convergence direction of NUVEL-1A (DeMets et al., 2010). Gray and blue lines in (a) are the original estimate and optimal solution of the moment rate function for this shallow VLFE. Observed, initial, and optimal waveforms in (b) and (c) are represented by gray solid, red dotted, and blue

dotted lines, respectively. Amplitudes at each station were normalized by the maximum amplitude of observed seismograms at frequencies of 0.02–0.05 Hz for each station.

3 Results

We evaluated 2,562 shallow VLFEs from April 2004 to January 2021 (Figure S9). The relationship between seismic moment and duration is illustrated in Figure 3. The results for different VR thresholds are plotted in Figures S5 and S6. Our results (Figure 3b) roughly followed the scaling relations of the slow earthquake family (including LFE, VLFE, and SSE) (e.g., Ide et al., 2007). Sugioka et al., 2012 and Takemura, Matsuzawa, et al. (2019) also estimated the seismic moments and durations of shallow VLFEs in the same region (Figure 3a). Moreover, our estimates (especially those with VRs ≥ 50 %) agreed with those of Sugioka et al., 2012) but were systematically larger than those of Takemura, Matsuzawa, et al. (2019). The assumption of a single pulse with various durations was applied in our previous study (Takemura et al., 2018; Takemura, Matsuzawa, et al., 2019). On the other hand, Sugioka et al. (2012) estimated the moment rate functions of shallow VLFEs from temporal ocean bottom seismometer data using a method based on the multiple-pulse assumption. This indicates that the estimation method of moment rate functions based on the single-pulse assumption can capture the centroid of the highest moment release but neglects minor sub-events (Figure S10). Thus, the optimal solutions based on the single-pulse assumption could not reproduce the observed later phases (red lines in Figure S10).

In addition, Takemura, Matsuzawa, et al. (2019) conducted centroid moment tensor inversions of shallow VLFEs at every 0.1° source grid without cross-correlation-based relocation. The 4D-grid (space and time) search CMT inversion generally includes the trade-off between locations and origin times. Thus, locations of shallow VLFEs in Takemura, Matsuzawa, et al. (2019) were widely scattered, and some of shallow VLFEs were located very close to the trench. The locations of shallow VLFEs in our catalog are improved compared with the catalog of Takemura, Matsuzawa, et al. (2019). Based on correlation analysis same as in this study, Takemura, Noda, et al. (2019) provided precise shallow VLFE locations in major episodes. However, their catalog was limited in the relatively large episodes and provided only shallow VLFE locations and counts. Thus, our long-term shallow VLFE catalog, including moment rate functions, can provide the opportunity to compare shallow VLFE moment release with tectonic environments in this region precisely.

The estimated durations should be equal to or shorter than 123 s due to limitations of our method. Although sharp boundary at a duration of 123 s was confirmed in Figure 3b, shallow VLFEs with durations of 20-60 s were dominant in our catalog. The amplitudes of surface waves are dominantly controlled by moment rates of shallow VLFEs. Thus, VRs of shallow VLFEs with smaller seismic moments or longer durations tend to be low (Figure 3b). Figure 3c shows the size distribution plot of shallow VLFEs with VRs ≥ 30 % (1,938 events) assuming a power law (the Gutenberg-Richter law). The power law with a *b*-value of approximately one appeared within the *Mw* range of 3.7 to 4.1. The number of shallow VLFEs with *Mw* ≥ 4.1 decreased more rapidly with increasing *Mw*. The size distribution characteristics of shallow VLFEs did not change with different VR thresholds in the source time function estimates (Figures S5 and S6).

Obtained size distributions of shallow VLFEs with Mw ≥ 3.7 agreed with size distributions of shallow seismic slow earthquakes in this region (Nakano et al., 2019), which were obtained by analysis of tremors and VLFEs recorded at DONET ocean bottom seismometers. Thus, we think that our catalog stably contained shallow VLFEs with Mw ≥ 3.7.

Figure 4a shows the temporal variation in the cumulative moment of shallow VLFEs in the study region. Temporal variations of the cumulative moment from shallow VLFEs with different thresholds (85 % and 95 % of the VR_m) are shown in Figure S7. Owing to template matching and moment rate function estimation based on the multi-pulse assumption, the cumulative moments of the new shallow VLFE catalog were larger than those of Takemura, Matsuzawa, et al. (2019). The total seismic moment released by 17 years of shallow VLFE activity was 2.69×10^{18} Nm (*Mw* 6.2). Figure 4b shows the spatiotemporal variations of shallow VLFE epicenters along X–X' (strike, 59º from the north) and Y-Y' (dip) directions. We identified three major episodes (≥ 200 shallow VLFEs over a wide area) that started from September 2004, March 2009, and December 2020, respectively. Other minor episodes (≥ 10 shallow VLFEs in a limited area) occurred in August 2005, July 2007, March 2008, April 2016, and May 2018. Here, we focus on variations in shallow VLFE activities in the along-strike direction (along X–X' in Figure 4b). Around X of −60 km to −20 km along this section, south-southeast off the Kii Peninsula, shallow VLFEs rarely occurred. In contrast, in regions > 0 km, shallow VLFEs actively occurred. The moment rates of shallow VLFEs in these regions were larger than those in the regions with X < -20 km. Such along-strike variations are illustrated in Figure 5. Along strike variation of cumulative moments due shallow VLFEs is similar in our previous study (Takemura, Matsuzawa, et al., 2019). Our catalog includes the large episode from December 2020 and other minor activities from the template-matching analysis. In addition, due to relocation and moment rate function estimation, more quantitative discussions about the spatial variations of shallow VLFE actvitiy can be conducted. Figure 5a shows a map view of the cumulative number and moments of shallow VLFEs southeast off the Kii Peninsula. Figure 5b shows the along-strike variations in the durations and moment rates of individual shallow VLFEs. A value of 5×10^{12} Nm/s is suggested as the lowest moment rate of detectable shallow VLFEs at onshore F-net stations. In cases of shallow VLFEs with smaller moment rates, meaning smaller moment or longer duration, signals of surface waves become weak compared with nose signals, and consequently, the VRs of shallow VLFEs with moment rates less than approximately 5×10^{12} Nm/s could not be listed in our catalog. Similar spatial variations were also observed in the solution with 95 % VR_m (Figure S8).

Based on the along-strike variations of shallow VLFE characteristics, we divided the shallow VLFE activity into three regions: Region 1 (−60 km to −20 km), Region 2 (0–35 km), and Region 3 (35–70 km). In Region 1 (blue dashed rectangle and line), shallow VLFE activity was minor, and their moment rates ranged from 5×10^{12} Nm/s to 5×10^{13} Nm/s, which were smaller than those in the other two regions. The cumulative moments in Regions 2 and 3 are similar, but the cumulative number of shallow VLFEs is larger in the red dashed rectangle. The shallow VLFEs with larger (> 1×10^{14} Nm/s) moment rates are concentrated in X of 0-35 km (Figure 5b). Thus, we divided shallow VLFE active area into Regions 2 and 3. Detailed characteristics of Regions 2 and 3 are followings. In Region 2 (red dashed rectangle and line), the shallow VLFEs were the most active. Both the cumulative number and moments were the highest (1,011 and 1.47×10^{18} Nm, respectively). The maximum shallow VLFE moment rates were also the highest (approximately 2×10^{14} Nm/s) in this region. In Region 3 (purple dashed rectangle and line), shallow VLFE activity was also high, but the cumulative number and moments (856 and 1.14×10^{18} Nm) were slightly less than those in Region 2. The maximum moment rates were also slightly lower than those in Region 2.

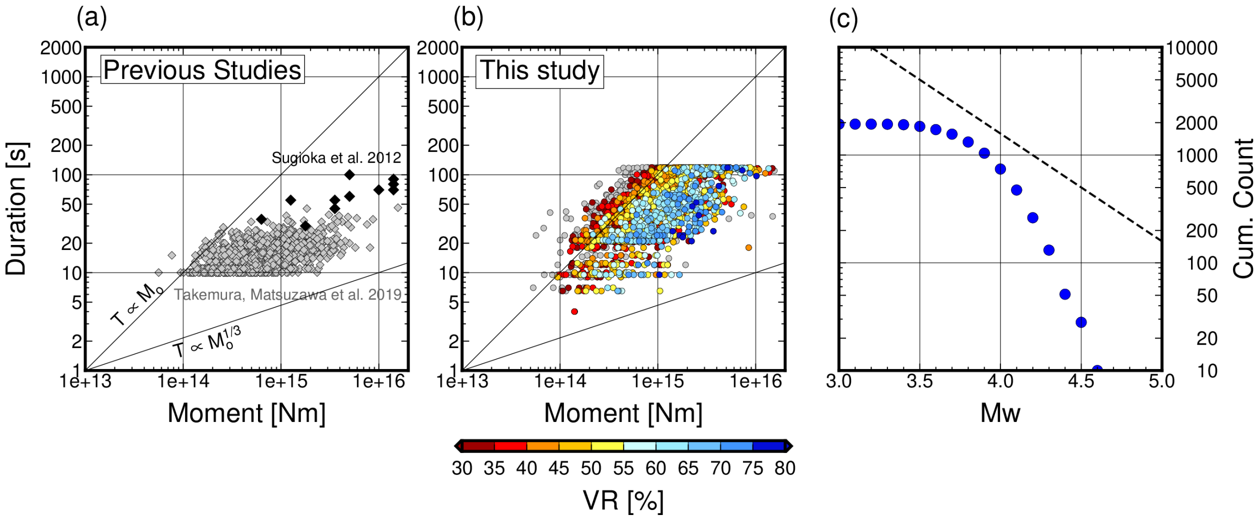

Figure 3. Relationship between seismic moments and durations of shallow VLFEs southeast off the Kii Peninsula. Black and gray diamonds in (a) represent the relationships between seismic moments and durations of shallow VLFEs in Sugioka et al. (2012) and Takemura, Matsuzawa, et al. (2019), respectively. Colors in (b) represent the values of VRs. (c) Size distribution of shallow VLFEs in this study, evaluated from shallow VLFEs with VRs ≥ 30 %. Dashed line in (c) represents the Gutenberg-Richter relationship with a *b*-value of 1.

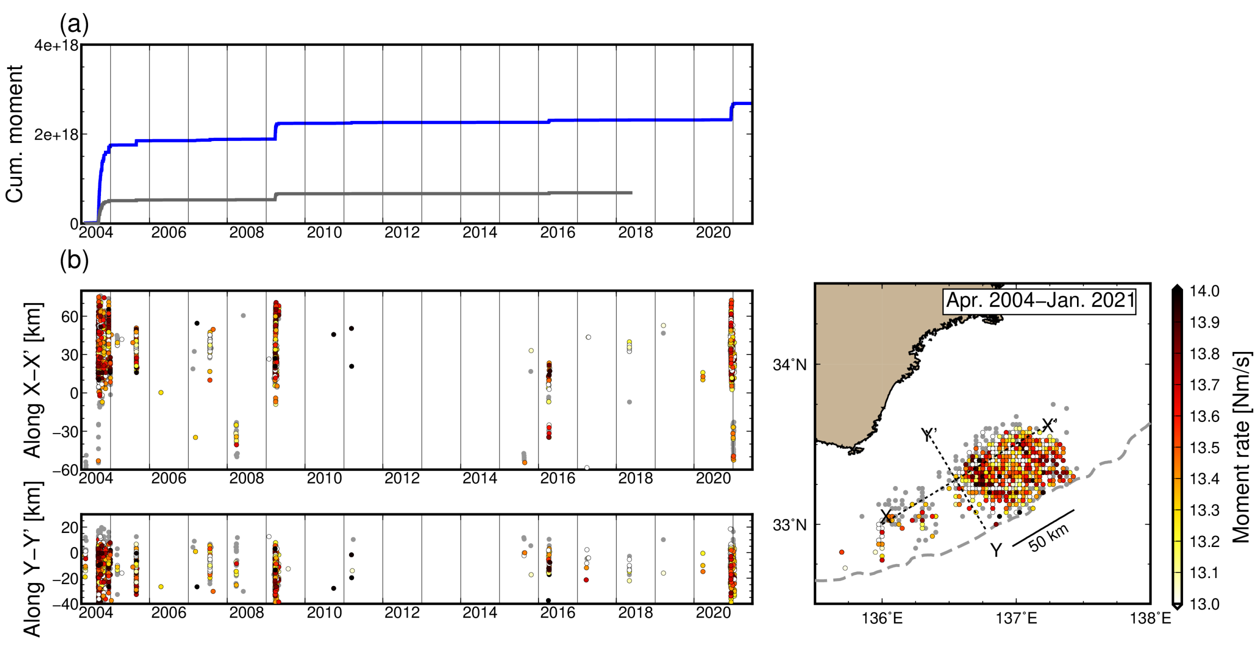

Figure 4. (a) Temporal variations of the cumulative moment and (b) spatiotemporal distribution of the moment rate of shallow VLFEs southeast off the Kii Peninsula. Gray and blue lines in (a) are the cumulative moments derived from the catalog in our previous study (Takemura, Matsuzawa, et al. (2019) and this study, respectively. Colors in (b) represent the seismic moments and moment rates of shallow VLFEs with VRs equal to or greater than 30 %. Gray

circles represent detected shallow VLFEs with VRs less than 30 %. The intersection point between X-X' and Y-Y' represents X = 0 km and Y = 0 km.

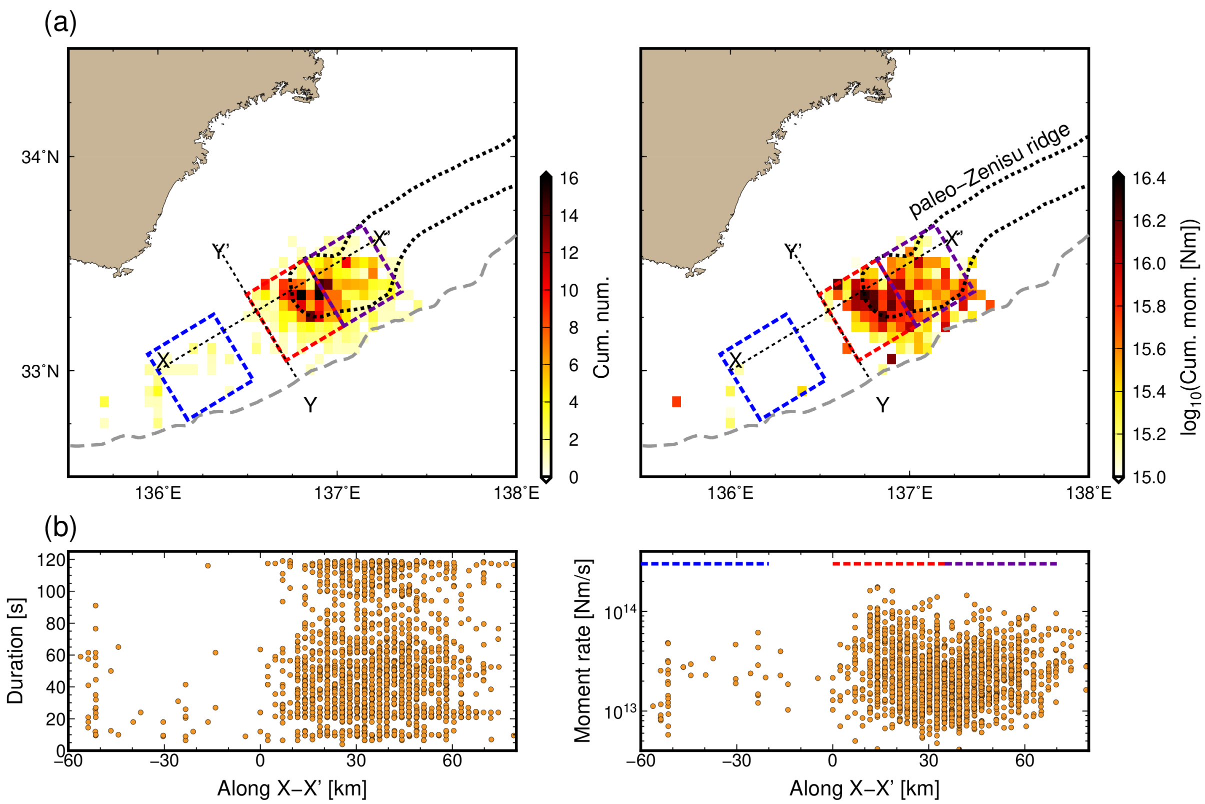

Figure 5. (a) Spatial variations of the block mean values of the cumulative number and moments of shallow VLFEs. We conducted spatial smoothing of the cumulative number and moments of shallow VLFEs within the region of 0.05º×0.05º on the map via the gridding algorithm provided by Generic Mapping Tools (Wessel et al., 2013). Blue, red, and purple dashed rectangles represent Regions 1, 2, and 3, respectively. (b) Along-strike variations in the durations and moment rate of individual shallow VLFEs. Black dotted line represents the location of the paleo-Zenisu ridge (Park et al., 2002, 2004), which is the subducted ridge beneath the study area.

4. Discussion

4.1. Spatial variations of slip behavior on the plate boundary inferred from the estimated source time functions of shallow VLFEs

Various offshore seismic surveys and analysis of DONET waveforms revealed detailed subsurface structures beneath southeast off the Kii Peninsula (e.g., Akuhara et al., 2020; Park et al., 2002, 2004; Tonegawa et al., 2017; Yamamoto et al., 2017). The large coseismic slip of past earthquakes and the spatial variation of interseismic locking in the Nankai Trough have been well studied (e.g., Murotani et al., 2015; Noda et al., 2018). Comparisons with such studies could provide key information for resolving the causes of along-strike variations in shallow VLFE activity in this region. Thus, in this subsection, we compare the observed along-strike variations of shallow VLFE activity with the tectonic environments in this region.

The pore-fluid pressure condition around the plate boundary is an important factor for slow earthquake activity (e.g., Delph et al., 2018; Nakajima & Hasegawa, 2016; Saffer & Wallace, 2015). The pore-fluid pressure is expected to be high within low-velocity volume (e.g., Kitajima & Saffer, 2012). Around regions with strong locking or low pore-fluid pressure, shallow slow earthquakes also tend to be less active (e.g., Baba et al., 2020; Dixon et al., 2014; Nishikawa et al., 2019). The subducted seamount was not imaged in Region 1 (e.g., Park et al., 2002, 2004). Thus, low shallow VLFE activity in Region 1 may be linked to low pore-fluid pressure conditions expected from velocity structures around the plate boundary (e.g., Tonegawa et al., 2017; Yamamoto et al., 2017) and strong interplate locking (e.g., Noda et al., 2018). Based on the observed interplate locking distribution in Nankai, Noda et al. (2021) constructed rupture scenario models for anticipated megathrust earthquakes. In these scenario models, large stress drops and coseismic slips were expected around Region 1. Thus, we consider that shallow slow earthquakes in Region 1 may have a minor contribution to the release of accumulated shear stress due to the subduction of the Philippine Sea Plate.

In Regions 2 and 3, shallow VLFE activity is high. Zones with high V_P/V_S ratios are commonly imaged around the plate boundary (e.g., Akuhara et al., 2020; Tonegawa et al., 2017), indicating that high pore-fluid pressure conditions are expected beneath these regions. Based on multichannel seismic (MCS) reflection profiles (Park et al., 2002, 2004), the paleo-Zenisu ridge (subducted ridge; black dotted line in Figure 5) was confirmed in both Regions 2 and 3. In addition, a décollement zone along the plate boundary was also confirmed beneath the western side of Region 2 from the MCS profile of Park et al. (2002). Thus, a significant change in the geometry of the subducting Philippine Sea Plate exists in Region 2.

The relationship between the subducting ridge and slow earthquakes has been documented in various subduction zones (e.g., Kubo & Nishikawa, 2020; Sun et al., 2020; Todd et al., 2018). Toh et al. (2018, 2020) suggested that the paleo-Zenisu ridge is also related to shallow VLFE activity in this region. Although their analysis provided more precise locations of shallow VLFEs due to DONET data, our long-term shallow VLFEs are in good agreement with their results. Our shallow VLFE catalog additionally revealed the relationship between the cumulative moment releases due to long-term shallow VLFE activity and topographic features of the Philippine Sea Plate. Dehydrated fluid is also heterogeneously distributed around subducted seamounts (e.g., Chesley et al., 2021). The relationship between shallow slow earthquakes and pore pressure in the same region have also been discussed in previous studies (e.g., Akuhara et al., 2020; Kitajima & Saffer, 2012; Toh et al., 2018, 2020; Tonegawa et al., 2017; Yamamoto et al., 2022). Numerical studies (e.g., Ruh et al., 2016; Sun et al., 2020) revealed that the subducted seamount can reduce the effective normal stress in up-dip part of a subducted seamount and down-dip regions surrounding a seamount. Thus, we consider that the paleo-Zenisu ridge causes heterogeneous structure and stress conditions in Regions 2 and 3, which proposed by previous studies (Toh et al., 2018, 2020). These heterogeneous structural and stress conditions due to the paleo-Zenisu ridge promote large moment release due to shallow VLFEs. The slightly higher activity in Region 2 could be related to the significant change in the geometry of the subducting Philippine Sea Plate beneath Region 2 (Park et al., 2002, 2004).

4.2. Variations of shallow VLFE migrations southeast off the Kii Peninsula

According to offshore borehole observation data southeast off the Kii Peninsula, Araki et al., 2017 detected eight shallow SSEs from 2011 to 2016. Ariyoshi et al., 2021 also reported a shallow SSE in March 2020. According to their detections and our shallow VLFE catalog, we observed the simultaneous occurrence of shallow VLFEs and SSEs in March 2011, October 2015, April 2016, and March 2020. Because of the spatiotemporal limitations of offshore geodetic observations (e.g., Araki et al., 2017; Yokota & Ishikawa, 2020), the detailed rupture processes of shallow SSEs cannot be resolved. The migration of tremors and VLFEs may be linked to the rupture processes of SSEs (e.g., Bartlow et al., 2011; Hirose & Obara, 2006; Ito et al., 2007; Rogers & Dragert, 2003). In this subsection, we investigate the spatiotemporal characteristics of shallow VLFE episodes in order to evaluate the possible shallow SSE rupture processes southeast off the Kii Peninsula.

Because our relocated epicenters have relatively large uncertainties along the dip direction owing to the station distribution (Figure 1), we focused our attention on migration patterns along the strike direction. The along-strike migration patterns of shallow VLFE episodes are illustrated in Figures 6, S11, and S12. The episode from September 2004 (Figure S11) was the largest; however, the complicated spatiotemporal variations of shallow VLFEs in this episode might have been affected by the *Mw* 7.4 intraplate earthquake and resulting afterslip that occurred on 5 September, 2004 (e.g., Watanabe et al., 2018). Figure 6 shows the migrations of shallow VLFEs in the episodes that started from March 2009 and December 2020. The cumulative moments during these two episodes were very similar (3.53×10^{17} and 3.67×10^{17} Nm, respectively). Shallow VLFEs with high moment rates were concentrated along the main migration fronts, and several rapid reverse migrations occurred in both episodes (left panels of Figure 6). The rapid migrations of shallow VLFEs occurred on 3 April 2009, 8 April 2009, and 28 December 2020. The speed of the observed reverse migrations was approximately 35-60 km/day, which was slightly slower than the rapid reverse migration of shallow slow earthquakes observed in the Hyuga-nada region (100–200 km/day; Asano et al., 2015; Yamashita et al., 2015). In the episode from March 2009 (upper panel of Figure 6), shallow VLFE activity initiated at approximately 10 km along X–X’, and then migrated eastward along the strike direction at a speed of approximately 8 km/day, which is close to the typical migration speeds of the major fronts of shallow slow earthquakes in other regions (e.g., Tanaka et al., 2019) and deep slow earthquakes (e.g., Houston et al., 2011; Obara, 2010). On the other hand, in the episode from December 2020, shallow VLFE activity initiated at approximately 40 km along X–X’, and then bilaterally migrated along the strike direction at a speed of approximately 4 km/day. This activity extended south-southeast off the Kii Peninsula (-50 km along X–X’).

We can catch the initiation locations and activity areas of each shallow VLFE episode from Figure 7. The spatiotemporal variations of other minor episodes are illustrated in Figure S12. The shallow VLFEs during the major episodes were commonly concentrated within the same active area (Regions 2 and 3; left panel of Figure 7), although the migration directions and initiation locations in the episode from December 2020 were different. On the other hand, the activity areas of minor episodes, except for that in March 2008, exhibited distinct locations within a part of the major activity area (right part of Figure 7). Shallow VLFEs during three minor episodes (August 2005, July 2007, and May 2018) migrated or clustered within the western edge of the paleo-Zenisu Ridge. In other words, minor episodes were limited within the western edge of the paleo-Zenisu Ridge (black dotted line in Figure 7). The episode in April 2016, which could be considered as triggered episode by the afterslip of the *Mw* 5.9 interplate earthquake (e.g., Wallace et al., 2016), mostly shared the western part of the activity areas of major episodes. The shallow VLFEs in April 2016 could not be found in the western edge of the paleo-Zenisu Ridge. The paleo-Zenisu Ridge or surrounding structures play a role as a barrier for minor episodes. To investigate these possibilities, a more precise shallow VLFE location technique or structural information should be required.

By applying the ambient noise monitoring technique to DONET data from August 2011 to March 2021 (diamonds in Figure 7), Tonegawa et al. (2021) investigated the temporal change of Green’s functions for each station pair. The cross-correlation functions of ambient noise records at each station pair can be considered as Green’s functions of each station pair. They found temporal changes of Green’s functions before/during shallow slow earthquakes. They interpreted that these changes might be caused by heterogeneous structure change due to fluid migration from the subducting plate, which reduced the effective stress on the plate boundary and promoted the rupture of shallow slow earthquakes. They also imaged the area with heterogeneous structure change. The area exhibiting heterogeneous structural changes in the episode from December 2020 (Tonegawa et al., 2021) agreed well with the area of shallow VLFE activity. Accordingly, we consider that the observed spatiotemporal variations of shallow VLFEs may reflect fluid migration during shallow SSEs in each episode. Tonegawa et al. (2021) also illustrated various heterogeneous change patterns associated with shallow slow earthquakes. According to their heterogeneous change and our shallow VLFEs in the episode from December 2020, pore fluid and/or rupture front of shallow SSE might propagate from the paleo-Zenisu ridge to the west. Thus, we interpret that observed variations in the initiation location, migration direction, and area of shallow VLFE episodes reflect temporal changes in the heterogeneous distribution of pore fluid or shear stress on the plate boundary. The heterogeneous temporal activity patterns during minor episodes were also affected by subduction of the paleo-Zenisu ridge. For a more detailed discussion of these processes, future studies should employ high-resolution topographic data of the subducting Philippine Sea Plate and 3D subsurface velocity structure models.

The ambient noise monitoring method at DONET stations is a direct and powerful tool for monitoring fluid migration on the plate boundary; however, the temporal resolution of this method is not high (> one month), compared to the typical durations of shallow slow earthquake episodes (several days to months). In addition, due to the observation period, DONET recorded only one major episode from December 2020 and several minor episodes. Thus, the detailed process of fluid migration during slow earthquakes cannot be fully resolved using this technique. Our spatiotemporal distributions of shallow VLFE migrations (Figures 6, S11, and S12) can more effectively resolve the detailed process of SSE rupture and fluid migration around the plate boundary. Continuous monitoring and more sophisticated methods for analyzing shallow slow earthquake signals and resolving locations in the along-dip direction can resolve the complexities of these processes in future studies.

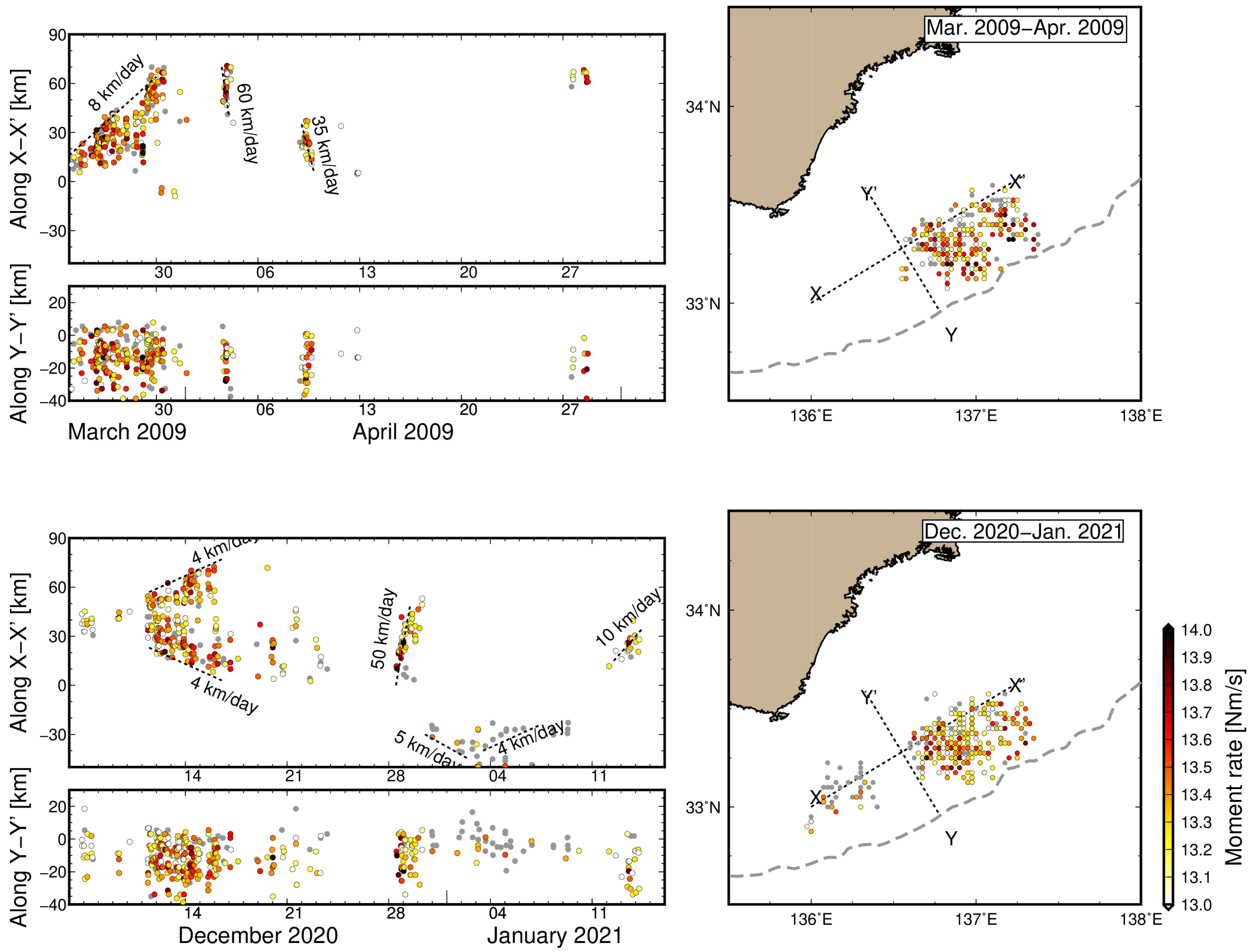

Figure 6. Spatiotemporal distributions of shallow VLFEs during the episodes from (a) March 2009 and (b) December 2020. Colors represent the seismic moments and moment rates of shallow VLFE with VRs ≥ 30 %.

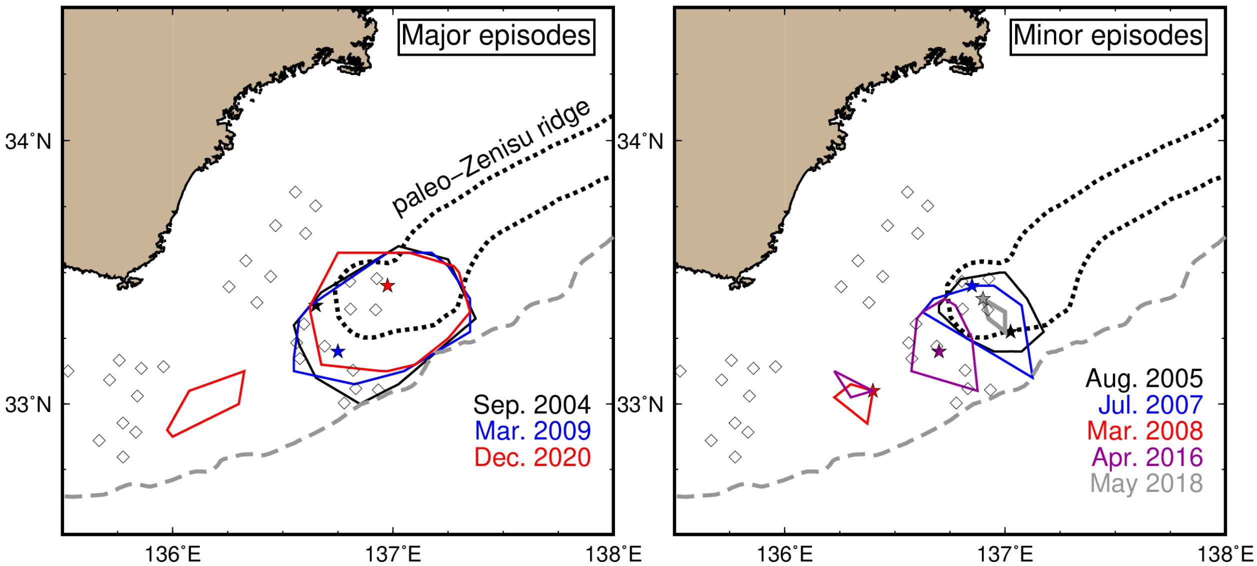

Figure 7. Shallow VLFE activity patterns southeast off the Kii Peninsula. Activity areas are defined by the convex hull of the relocated shallow VLFE epicenters in each episode. Stars indicate the epicenter of the initial shallow VLFE in each episode. Black dotted line represents the location of the paleo-Zenisu ridge (Park et al., 2002, 2004). Diamonds represent the locations of DONET stations.

5. Conclusions

Template matching and relocation based on cross-correlation analysis of onshore broadband records were employed to comprehensively detect shallow VLFEs southeast off the Kii Peninsula along the Nankai Trough. Based on the relocated shallow VLFE locations, we estimated their source time functions using Green's functions in the local 3D model. The estimated source characteristics of shallow VLFEs revealed their spatiotemporal activity patterns in this region. Shallow VLFEs were widely distributed around the accretionary prism toe but exhibited large cumulative moments in the region around the western edge of the subducted paleo-Zenisu ridge. This observation suggests that the heterogeneous structure and stress conditions caused by the subduction of the paleo-Zenisu ridge cause large moment release of shallow VLFEs in this region.

The relocated epicenters illustrated the along-strike migration of shallow VLFEs during three major episodes characterized by a similar activity area and five minor episodes with various activity areas. The major episodes exhibited slow frontal migration with different initiation locations, migration directions, and migration speeds and included several rapid reverse migrations. Minor episodes were distributed in distinct areas within a part of the major episode activity area. According to the characteristics of shallow VLFE episodes and the plate geometry in previous studies, the subducted ridge also plays a barrier for minor shallow VLFE episodes. Recent developments in monitoring heterogeneous changes from ambient noise wavefields have imaged various areas of heterogeneous change associated with shallow slow earthquakes. Therefore, we conclude that the various migration patterns of shallow VLFE episodes (activity area, speed, and direction) are caused by temporal changes in the pore-fluid pressure or stress conditions on the plate boundary. As such, shallow VLFE monitoring can be an important indicator of these processes.

Acknowledgments

Numerical simulations for evaluating Green's functions were conducted using the Fujitsu PRIMERGY CX600M1/CX1640M1 (Oakforest-PAC) at the Information Technology Center, University of Tokyo. This study was supported by a JSPS KAKENHI Grant-in-Aid for Scientific Research (C), grant number 21K03696, and a Grant-in-Aid for Scientific Research on Innovative Areas "Science of slow earthquakes," grant numbers 19H04626 and JP16H06473. This study was also supported by ERI JURP 2020-S-04 and 2021-S-B102, which provided computational resources for calculating Green's functions. We thank Akiko Takeo, Yojiro Yamamoto, Takashi Tonegawa, Kojiro Tamaribuchi, Masashi Ogiso, Ryo Okuwaki, Takanori Matsuzawa, Akemi Noda, and Kentaro Emoto for useful discussions. We also acknowledge two anonymous reviewers, the associate editor and editor Prof. Y. Ben-Zion, for careful reviewing and constructive comments, which helped to improve the manuscript.

Data availability statement

The Python package HinetPy (Tian, 2020) was used to download NIED F-net continuous records (National Research Institute for Earth Science and Disaster Resilience, 2019). The catalogs of shallow VLFEs from previous studies (Sugioka et al., 2012; Takemura, Matsuzawa, et al., 2019) were downloaded from the Slow Earthquake Database website (Kano et al., 2018; http://www-solid.eps.s.u-tokyo.ac.jp/~sloweq/). We simulated Green's functions in the local 3D model using OpenSWPC version 5.1.0 https://doi.org/10.5281/zenodo.3982232. The 1D layered velocity models of Tonegawa et al., 2017) can be downloaded from https://doi.org/10.5281/zenodo.4158947. The JIVSM (Koketsu et al., 2012) was obtained from https://www.jishin.go.jp/evaluation/seismic_hazard_map/lpshm/12_choshuki_dat/. We used the Seismic Analysis Code (Goldstein & Snoke, 2005; Helffrich et al., 2013) and Generic Mapping Tools (Wessel et al., 2013) for signal processing and figure drawing. Some of the data analysis was conducted using NumPy (Harris et al., 2020), SciPy 1.7.0 (https://doi.org/10.5281/zenodo.5000479), and Pandas 1.2.5 (https://doi.org/10.5281/zenodo.5013202). The estimated moment rate functions of shallow VLFEs southeast off the Kii Peninsula can be downloaded from https://doi.org/10.5281/zenodo.5211090.

References

Agata, R. (2020). Introduction of covariance components in slip inversion of geodetic data following a non-uniform spatial distribution and application to slip deficit rate estimation in the Nankai Trough subduction zone. *Geophysical Journal International*, *221*(3), 1832–1844. https://doi.org/10.1093/gji/ggaa116

Akuhara, T., Tsuji, T., & Tonegawa, T. (2020). Overpressured Underthrust Sediment in the Nankai Trough Forearc Inferred From Transdimensional Inversion of High-Frequency Teleseismic Waveforms. *Geophysical Research Letters*, *47*(15), 0–3. https://doi.org/10.1029/2020GL088280

Ando, M. (1975). Source mechanisms and tectonic significance of historical earthquakes along the Nankai trough, Japan. *Tectonophysics*, *27*(2), 119–140. https://doi.org/10.1016/0040-1951(75)90102-X

Annoura, S., Hashimoto, T., Kamaya, N., & Katsumata, A. (2017). Shallow episodic tremor near the Nankai Trough axis off southeast Mie prefecture, Japan. *Geophysical Research Letters*, *44*(8), 3564–3571. https://doi.org/10.1002/2017GL073006

Aoi, S., Asano, Y., Kunugi, T., Kimura, T., Uehira, K., Takahashi, N., et al. (2020). MOWLAS: NIED observation network for earthquake, tsunami and volcano. *Earth, Planets and Space*, *72*(1). https://doi.org/10.1186/s40623-020-01250-x

Araki, E., Saffer, D. M., Kopf, A. J., Wallace, L. M., Kimura, T., Machida, Y., et al. (2017). Recurring and triggered slow-slip events near the trench at the Nankai Trough subduction megathrust. *Science*, *356*(6343), 1157–1160. https://doi.org/10.1126/science.aan3120

Ariyoshi, K., Iinuma, T., Nakano, M., Kimura, T., Araki, E., Machida, Y., et al. (2021). Characteristics of Slow Slip Event in March 2020 Revealed From Borehole and DONET Observatories. *Frontiers in Earth Science*, *8*. https://doi.org/10.3389/feart.2020.600793

Asano, Y., Obara, K., Matsuzawa, T., Hirose, H., & Ito, Y. (2015). Possible shallow slow slip events in Hyuga-nada, Nankai subduction zone, inferred from migration of very low frequency earthquakes, 331–338. https://doi.org/10.1002/2014GL062165.Received

Baba, S., Takemura, S., Obara, K., & Noda, A. (2020). Slow earthquakes illuminating interplate coupling heterogeneities in subduction zones. *Geophysical Research Letters*. https://doi.org/10.1029/2020GL088089

Baba, S., Obara, K., Takemura, S., Takeo, A., & Abers, G. A. (2021). Shallow Slow Earthquake Episodes Near the Trench Axis off Costa Rica. *Journal of Geophysical Research: Solid Earth*, *126*(9). https://doi.org/10.1029/2021JB021706

Bartlow, N. M., Miyazaki, S., Bradley, A. M., & Segall, P. (2011). Space-time correlation of slip and tremor during the 2009 Cascadia slow slip event. *Geophysical Research Letters*, *38*(18), 1–6. https://doi.org/10.1029/2011GL048714

Bostock, M. G., Thomas, A. M., Savard, G., Chuang, L., & Rubin, A. M. (2015). Magnitudes and moment-duration scaling of low-frequency earthquakes beneath southern Vancouver Island. *Journal of Geophysical Research B: Solid Earth*, *120*(9), 6329–6350. https://doi.org/10.1002/2015JB012195

Chesley, C., Naif, S., Key, K., & Bassett, D. (2021). Fluid-rich subducting topography generates anomalous forearc porosity. *Nature*, *595*(7866), 255–260. https://doi.org/10.1038/s41586-021-03619-8

Delph, J. R., Levander, A., & Niu, F. (2018). Fluid controls on the heterogeneous seismic characteristics of the Cascadia margin. *Geophysical Research Letters*. https://doi.org/10.1029/2018GL079518

DeMets, C., Gordon, R. G., & Argus, D. F. (2010). Geologically current plate motions. *Geophysical Journal International*, *181*(1), 1–80. https://doi.org/10.1111/j.1365-246X.2009.04491.x

Dixon, T. H., Jiang, Y., Malservisi, R., McCaffrey, R., Voss, N., Protti, M., & Gonzalez, V. (2014). Earthquake and tsunami forecasts: Relation of slow slip events to subsequent earthquake rupture. *Proceedings of the National Academy of Sciences*, *111*(48), 17039–17044. https://doi.org/10.1073/pnas.1412299111

Goldstein, P., & Snoke, A. (2005). SAC Availability for the IRIS Community. Retrieved from https://ds.iris.edu/ds/newsletter/vol7/no1/193/sac-availability-for-the-iris-community/

Harris, C. R., Millman, K. J., van der Walt, S. J., Gommers, R., Virtanen, P., Cournapeau, D., et al. (2020). Array programming with NumPy. *Nature*, *585*(7825), 357–362. https://doi.org/10.1038/s41586-020-2649-2

Helffrich, G., Wookey, J., & Bastow, I. (2013). *The Seismic Analysis Code*. Cambridge: Cambridge University Press. https://doi.org/10.1017/CBO9781139547260

Hirose, H., & Obara, K. (2006). Short-term slow slip and correlated tremor episodes in the Tokai region, central Japan. *Geophysical Research Letters*, *33*(17), L17311. https://doi.org/10.1029/2006GL026579

Houston, H., Delbridge, B. G., Wech, A. G., & Creager, K. C. (2011). Rapid tremor reversals in Cascadia generated by a weakened plate interface. *Nature Geoscience*, *4*(6), 404–409. https://doi.org/10.1038/ngeo1157

Ide, S., Beroza, G. C., Shelly, D. R., & Uchide, T. (2007). A scaling law for slow earthquakes. *Nature*, *447*(7140), 76–79. https://doi.org/10.1038/nature05780

Ide, S., Imanishi, K., Yoshida, Y., Beroza, G. C., & Shelly, D. R. (2008). Bridging the gap between seismically and geodetically detected slow earthquakes. *Geophysical Research Letters*, *35*(10), 2–7. https://doi.org/10.1029/2008GL034014

Ito, Y., Obara, K., Shiomi, K., Sekine, S., & Hirose, H. (2007). Slow earthquakes coincident with episodic tremors and slow slip events. *Science*, *315*(5811), 503–506. https://doi.org/10.1126/science.1134454

Kaneko, L., Ide, S., & Nakano, M. (2018). Slow Earthquakes in the Microseism Frequency Band (0.1-1.0 Hz) off Kii Peninsula, Japan. *Geophysical Research Letters*, *45*(6), 2618–2624. https://doi.org/10.1002/2017GL076773

Kano, M., Aso, N., Matsuzawa, T., Ide, S., Annoura, S., Arai, R., et al. (2018). Development of a slow earthquake database. *Seismological Research Letters*, *89*(4), 1566–1575. https://doi.org/10.1785/0220180021

Kato, A., Obara, K., Igarashi, T., Tsuruoka, H., Nakagawa, S., & Hirata, N. (2012). Propagation of slow slip leading up to the 2011 Mw9.0 Tohoku-Oki earthquake. *Science*, *335*(6069), 705–708. https://doi.org/10.1126/science.1215141

Kato, A., Fukuda, J., Kumazawa, T., & Nakagawa, S. (2016). Accelerated nucleation of the 2014 Iquique, Chile Mw 8.2 Earthquake. *Scientific Reports*, *6*(1), 24792. https://doi.org/10.1038/srep24792

Kitajima, H., & Saffer, D. M. (2012). Elevated pore pressure and anomalously low stress in regions of low frequency earthquakes along the Nankai Trough subduction megathrust. *Geophys. Res. Lett.*, *39*, 1–5. https://doi.org/10.1029/2012GL053793

Koketsu, K., Miyake, H., & Suzuki, H. (2012). Japan Integrated Velocity Structure Model Version 1. *Proceedings of the 15th World Conference on Earthquake Engineering*, 1–4. Retrieved from http://www.iitk.ac.in/nicee/wcee/article/WCEE2012_1773.pdf

Kubo, H., & Nishikawa, T. (2020). Relationship of preseismic, coseismic, and postseismic fault ruptures of two large interplate aftershocks of the 2011 Tohoku earthquake with slow-earthquake activity. *Scientific Reports*, *10*(1), 12044. https://doi.org/10.1038/s41598-020-68692-x

Maeda, T., Takemura, S., & Furumura, T. (2017). OpenSWPC: an open-source integrated parallel simulation code for modeling seismic wave propagation in 3D heterogeneous viscoelastic media. *Earth, Planets and Space*, *69*(1), 102. https://doi.org/10.1186/s40623-017-0687-2

Michel, S., Gualandi, A., & Avouac, J. (2019). Similar scaling laws for earthquakes and Cascadia slow-slip events. *Nature*, *574*(7779), 522–526. https://doi.org/10.1038/s41586-019-1673-6

Murotani, S., Shimazaki, K., & Koketsu, K. (2015). Rupture process of the 1946 Nankai earthquake estimated using seismic waveforms and geodetic data. *Journal of Geophysical Research : Solid Earth*, *120*, 5677–5692. https://doi.org/10.1002/2014JB011676

Nakajima, J., & Hasegawa, A. (2016). Tremor activity inhibited by well-drained conditions above a megathrust. *Nature Communications*, *7*, 13863. https://doi.org/10.1038/ncomms13863

Nakamura, T., Takenaka, H., Okamoto, T., Ohori, M., & Tsuboi, S. (2015). Long-period ocean-bottom motions in the source areas of large subduction earthquakes. *Scientific Reports*, *5*, 1–2. https://doi.org/10.1038/srep16648

Nakano, M., Hori, T., Araki, E., Kodaira, S., & Ide, S. (2018). Shallow very-low-frequency earthquakes accompany slow slip events in the Nankai subduction zone. *Nature Communications*, *9*(1), 984. https://doi.org/10.1038/s41467-018-03431-5

Nakano, M., Yabe, S., Sugioka, H., Shinohara, M., & Ide, S. (2019). Event Size Distribution of Shallow Tectonic Tremor in the Nankai Trough. *Geophysical Research Letters*, *46*(11), 5828–5836. https://doi.org/10.1029/2019GL083029

National Research Institute for Earth Science and Disaster Resilience. (2019). NIED F-net. https://doi.org/10.17598/NIED.0005

Nishida, K. (2017). Ambient seismic wave field. *Proceedings of the Japan Academy, Series B*, *93*(7), 423–448. https://doi.org/10.2183/pjab.93.026

Nishikawa, T., Matsuzawa, T., Ohta, K., Uchida, N., Nishimura, T., & Ide, S. (2019). The slow earthquake spectrum in the Japan Trench illuminated by the S-net seafloor observatories. *Science*, *365*(August), 808–813. https://doi.org/10.1126/science.aax5618

Noda, A., Saito, T., & Fukuyama, E. (2018). Slip-Deficit Rate Distribution Along the Nankai Trough, Southwest Japan, With Elastic Lithosphere and Viscoelastic Asthenosphere. *Journal of Geophysical Research: Solid Earth*, *123*(9), 8125–8142. https://doi.org/10.1029/2018JB015515

Noda, A., Saito, T., Fukuyama, E., & Urata, Y. (2021). Energy-Based Scenarios for Great Thrust-Type Earthquakes in the Nankai Trough Subduction Zone, Southwest Japan, Using an Interseismic Slip-Deficit Model. *Journal of Geophysical Research: Solid Earth*, *126*(5). https://doi.org/10.1029/2020JB020417

Obara, K. (2010). Phenomenology of deep slow earthquake family in southwest Japan: Spatiotemporal characteristics and segmentation. *Journal of Geophysical Research: Solid Earth*, *115*(8), 1–22. https://doi.org/10.1029/2008JB006048

Obara, K., & Ito, Y. (2005). Very low frequency earthquakes excited by the 2004 off the Kii peninsula earthquakes: A dynamic deformation process in the large accretionary prism. *Earth, Planets and Space*, *57*(4), 321–326. https://doi.org/10.1186/BF03352570

Obara, K., & Kato, A. (2016). Connecting slow earthquakes to huge earthquakes. *Science*, *353*(6296), 253–257. https://doi.org/10.1126/science.aaf1512

Park, J.-O., Tsuru, T., Kodaira, S., Cummins, P. R., & Kaneda, Y. (2002). Splay fault branching along the Nankai subduction zone. *Science*, *297*(5584), 1157–1160. https://doi.org/10.1126/science.1074111

Park, J.-O., Moore, G. F., Tsuru, T., Kodaira, S., & Kaneda, Y. (2004). A subducted oceanic ridge influencing the Nankai megathrust earthquake rupture. *Earth and Planetary Science Letters*, *217*(1–2), 77–84. https://doi.org/10.1016/S0012-821X(03)00553-3

Plata-Martinez, R., Ide, S., Shinohara, M., Garcia, E. S., Mizuno, N., Dominguez, L. A., et al. (2021). Shallow slow earthquakes to decipher future catastrophic earthquakes in the Guerrero seismic gap. *Nature Communications*, *12*(1), 3976. https://doi.org/10.1038/s41467-021-24210-9

Rogers, G., & Dragert, H. (2003). Episodic tremor and slip on the Cascadia subduction zone: the chatter of silent slip. *Science*, *300*(5627), 1942–1943. https://doi.org/10.1126/science.1084783

Ruh, J. B., Sallarès, V., Ranero, C. R., & Gerya, T. (2016). Crustal deformation dynamics and stress evolution during seamount subduction: High-resolution 3-D numerical modeling. *Journal of Geophysical Research: Solid Earth*, *121*(9), 6880–6902. https://doi.org/10.1002/2016JB013250

Saffer, D. M., & Wallace, L. M. (2015). The frictional, hydrologic, metamorphic and thermal habitat of shallow slow earthquakes. *Nature Geoscience*, *8*(8), 594–600. https://doi.org/10.1038/ngeo2490

Sugioka, H., Okamoto, T., Nakamura, T., Ishihara, Y., Ito, A., Obana, K., et al. (2012). Tsunamigenic potential of the shallow subduction plate boundary inferred from slow seismic slip. *Nature Geoscience*, *5*(6), 414–418. https://doi.org/10.1038/ngeo1466

Sun, T., Saffer, D., & Ellis, S. (2020). Mechanical and hydrological effects of seamount subduction on megathrust stress and slip. *Nature Geoscience*, *13*(March). https://doi.org/10.1038/s41561-020-0542-0

Supino, M., Poiata, N., Festa, G., Vilotte, J. P., Satriano, C., & Obara, K. (2020). Self-similarity of low-frequency earthquakes. *Scientific Reports*, *10*(1), 1–9. https://doi.org/10.1038/s41598-020-63584-6

Takemura, S., Matsuzawa, T., Kimura, T., Tonegawa, T., & Shiomi, K. (2018). Centroid Moment Tensor Inversion of Shallow Very Low Frequency Earthquakes Off the Kii Peninsula, Japan, Using a Three-Dimensional Velocity Structure Model. *Geophysical Research Letters*, *45*(13), 6450–6458. https://doi.org/10.1029/2018GL078455

Takemura, S., Noda, A., Kubota, T., Asano, Y., Matsuzawa, T., & Shiomi, K. (2019). Migrations and Clusters of Shallow Very Low Frequency Earthquakes in the Regions Surrounding Shear Stress Accumulation Peaks Along the Nankai Trough. *Geophysical Research Letters*, *46*(21), 11830–11840. https://doi.org/10.1029/2019GL084666

Takemura, S., Matsuzawa, T., Noda, A., Tonegawa, T., Asano, Y., Kimura, T., & Shiomi, K. (2019). Structural Characteristics of the Nankai Trough Shallow Plate Boundary Inferred From Shallow Very Low Frequency Earthquakes. *Geophysical Research Letters*, *46*(8), 4192–4201. https://doi.org/10.1029/2019GL082448

Takemura, S., Okuwaki, R., Kubota, T., Shiomi, K., Kimura, T., & Noda, A. (2020). Centroid moment tensor inversions of offshore earthquakes using a three-dimensional velocity structure model: slip distributions on the plate boundary along the Nankai Trough. *Geophysical Journal International*, *222*(2), 1109–1125. https://doi.org/10.1093/gji/ggaa238

Takemura, S., Yabe, S., & Emoto, K. (2020). Modelling high-frequency seismograms at ocean bottom seismometers: effects of heterogeneous structures on source parameter estimation for small offshore earthquakes and shallow low-frequency tremors. *Geophysical Journal International*, *223*(3), 1708–1723. https://doi.org/10.1093/gji/ggaa404

Tanaka, S., Matsuzawa, T., & Asano, Y. (2019). Shallow Low-Frequency Tremor in the Northern Japan Trench Subduction Zone. *Geophysical Research Letters*, *46*(10), 5217–5224. https://doi.org/10.1029/2019GL082817

Tian, D. (2020). HinetPy: A Python package to request and process seismic waveform data from Hi-net. https://doi.org/10.5281/zenodo.3885779

Tocheport, A., Rivera, L., & Chevrot, S. (2007). A systematic study of source time functions and moment tensors of intermediate and deep earthquakes. *Journal of Geophysical Research: Solid Earth*, *112*(7), 1–22. https://doi.org/10.1029/2006JB004534

Todd, E. K., Schwartz, S. Y., Mochizuki, K., Wallace, L. M., Sheehan, A. F., Webb, S. C., et al. (2018). Earthquakes and Tremor Linked to Seamount Subduction During Shallow Slow Slip at the Hikurangi Margin, New Zealand. *Journal of Geophysical Research: Solid Earth*. https://doi.org/10.1029/2018JB016136

Toh, A., Chen, W. J., Takeuchi, N., Dreger, D. S., Chi, W. C., & Ide, S. (2020). Influence of a Subducted Oceanic Ridge on the Distribution of Shallow VLFEs in the Nankai Trough as Revealed by Moment Tensor Inversion and Cluster Analysis. *Geophysical Research Letters*, *47*(15), 0–3. https://doi.org/10.1029/2020GL087244

Toh, Akiko, Obana, K., & Araki, E. (2018). Distribution of very low frequency earthquakes in the Nankai accretionary prism influenced by a subducting-ridge. *Earth and Planetary Science Letters*, *482*(March 2011), 342–356. https://doi.org/10.1016/j.epsl.2017.10.062

Tonegawa, T., Araki, E., Kimura, T., Nakamura, T., Nakano, M., & Suzuki, K. (2017). Sporadic low-velocity volumes spatially correlate with shallow very low frequency earthquake clusters. *Nature Communications*, *8*(1), 2048. https://doi.org/10.1038/s41467-017-02276-8

Tonegawa, T., Takemura, S., Yabe, S., & Yomogida, K. (2021). Fluid migration before and during slow earthquakes in the shallow Nankai subduction zone. *Earth and Space Science Open Archieve* . https://doi.org/10.1002/essoar.10508646.1

Vaca, S., Vallée, M., Nocquet, J. M., Battaglia, J., & Régnier, M. (2018). Recurrent slow slip events as a barrier to the northward rupture propagation of the 2016 Pedernales earthquake (Central Ecuador). *Tectonophysics*, *724–725*(November 2017), 80–92. https://doi.org/10.1016/j.tecto.2017.12.012

Voss, N., Dixon, T. H., Liu, Z., Malservisi, R., Protti, M., & Schwartz, S. (2018). Do slow slip events trigger large and great megathrust earthquakes ? *Science Advances*, *4*(10), eaat8472.

Wallace, L. M., Araki, E., Saffer, D., Wang, X., Roesner, A., Kopf, A., et al. (2016). Near-field observations of an offshore Mw 6.0 earthquake from an integrated seafloor and subseafloor monitoring network at the Nankai Trough, southwest Japan. *Journal of Geophysical Research: Solid Earth*, *121*(11), 8338–8351. https://doi.org/10.1002/2016JB013417

Watanabe, S., Bock, Y., Melgar, D., & Tadokoro, K. (2018). Tsunami Scenarios Based on Interseismic Models Along the Nankai Trough, Japan, From Seafloor and Onshore

Geodesy. *Journal of Geophysical Research: Solid Earth*, *123*(3), 2448–2461. https://doi.org/10.1002/2017JB014799

Wessel, P., Smith, W. H. F., Scharroo, R., Luis, J., & Wobbe, F. (2013). Generic mapping tools: Improved version released. *Eos*, *94*(45), 409–410. https://doi.org/10.1002/2013EO450001

Yabe, S., Baba, S., Tonegawa, T., Nakano, M., & Takemura, S. (2021). Seismic energy radiation and along-strike heterogeneities of shallow tectonic tremors at the Nankai Trough and Japan Trench. *Tectonophysics*, *800*, 228714. https://doi.org/10.1016/j.tecto.2020.228714

Yamamoto, Y., Takahashi, T., Kaiho, Y., Obana, K., Nakanishi, A., Kodaira, S., & Kaneda, Y. (2017). Seismic structure off the Kii Peninsula, Japan, deduced from passive- and active-source seismographic data. *Earth and Planetary Science Letters*, *461*, 163–175. https://doi.org/10.1016/j.epsl.2017.01.003

Yamamoto, Y., Ariyoshi, K., Yada, S., Nakano, M., & Hori, T. (2022). Spatio-temporal distribution of shallow very-low-frequency earthquakes between December 2020 and January 2021 in Kumano-nada, Nankai subduction zone, detected by a permanent seafloor seismic network. *Earth, Planets and Space*, *74*(1), 14. https://doi.org/10.1186/s40623-022-01573-x

Yamashita, Y., Yakiwara, H., Asano, Y., Shimizu, H., Uchida, K., Hirano, S., et al. (2015). Migrating tremor off southern Kyushu as evidence for slow slip of a shallow subduction interface. *Science*, *348*(6235), 676–679. https://doi.org/10.1126/science.aaa4242

Yokota, Y., & Ishikawa, T. (2020). Shallow slow slip events along the Nankai Trough detected by GNSS-A. *Science Advances*, *6*(3), eaay5786. https://doi.org/10.1126/sciadv.aay5786

AGU PUBLICATIONS

Journal of Geophysical Research: Solid Earth

Supporting Information for

Spatiotemporal variations of shallow very low frequency earthquake activity southeast off the Kii Peninsula, along the Nankai Trough, Japan

Shunsuke TAKEMURA[1], Kazushige OBARA[1], Katsuhiko SHIOMI[2], and Satoru BABA[1]

[1]Earthquake Research Institute, the University of Tokyo, 1-1-1 Yayoi, Bunkyo-ku, Tokyo, 113-0032, Japan; [2]Network Center of Earthquake, Tsunami and Volcano, National Research Institute for Earth Science and Disaster Resilience, 3-1 Tennodai, Tsukuba, Ibaraki, 305-0006, Japan.

Contents of this file

Figures S1 to S12

Introduction

Spatial variations of cross correlation coefficients in the shallow VLFE relocation are illustrated in Figure S1. Figure S2 shows the temporal change in the cumulative number of detected shallow VLFEs. Comparisons of synthetic seismograms between the original and our optimal moment rate functions are shown in Figure S3. Figures S4–S7 illustrate the results with different VR thresholds. Temporal variations in the cumulative moments of shallow VLFEs with different thresholds are shown in Figure S8. The along-strike spatial variations of shallow VLFE activity from the catalog for 95 % of the VR_m (Figure S9) are similar to those in Figure 5. Figure S10 shows the comparison of the estimated moment rate functions of Takemura, Matsuzawa et al. (2018) with those of this study. Figures S11 and S12 show the spatiotemporal variations of shallow VLFE episodes that started in September 2004, August 2005, July 2007, March 2008, and April 2016.

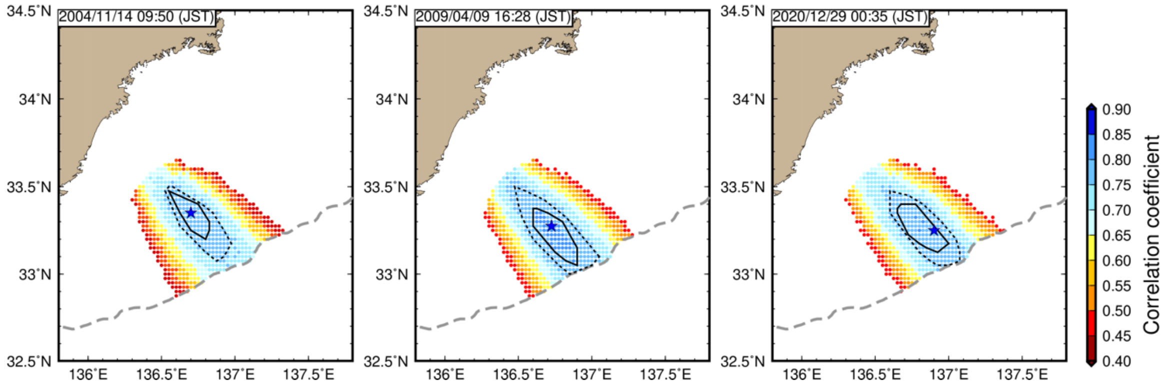

Figure S1. Examples of spatial distributions of cross correlation coefficients in shallow VLFE relocation. Maximum average cross correlation coefficients at each grid for 1 min of the optimal origin time are plotted. The blue stars are the optimal epicenters of shallow VLFEs occurred at 09:50 on 14 November 2004 (JST), 16:28 on 9 April 2009 (JST), and 00:35 on 29 December 2020 (JST). The enclosed areas by black solid and dotted lines are the convex-hulls of shallow VLFEs with CCs equal to or greater than 95 % and 98 % of maximum correlation coefficients. In these plots, we discarded grid points with maximum correlation coefficients less than 0.45 (detection threshold).

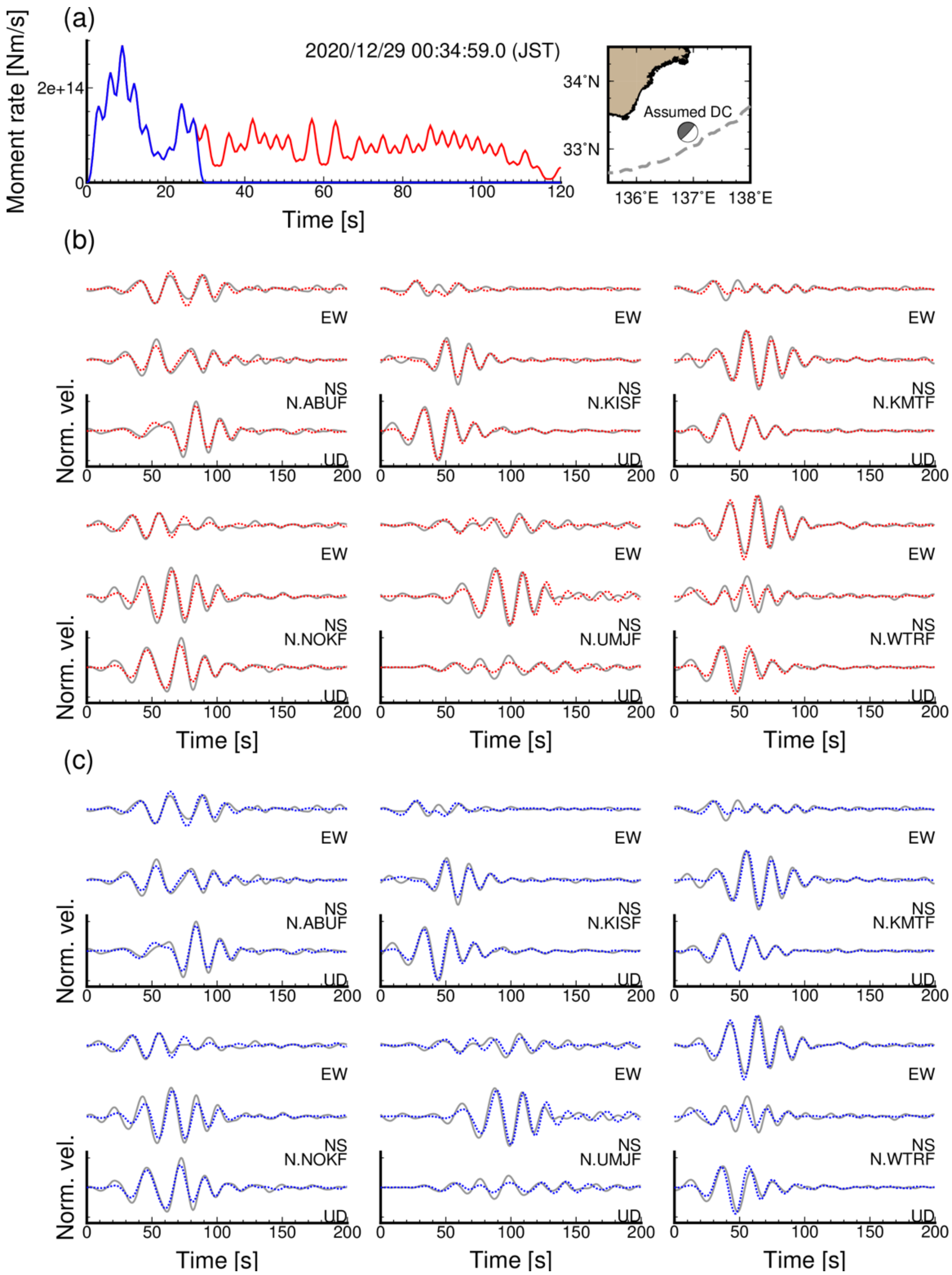

Figure S2. Same as Figure 2 but red lines indicate synthetic seismograms from the original result of our simulated annealing method.

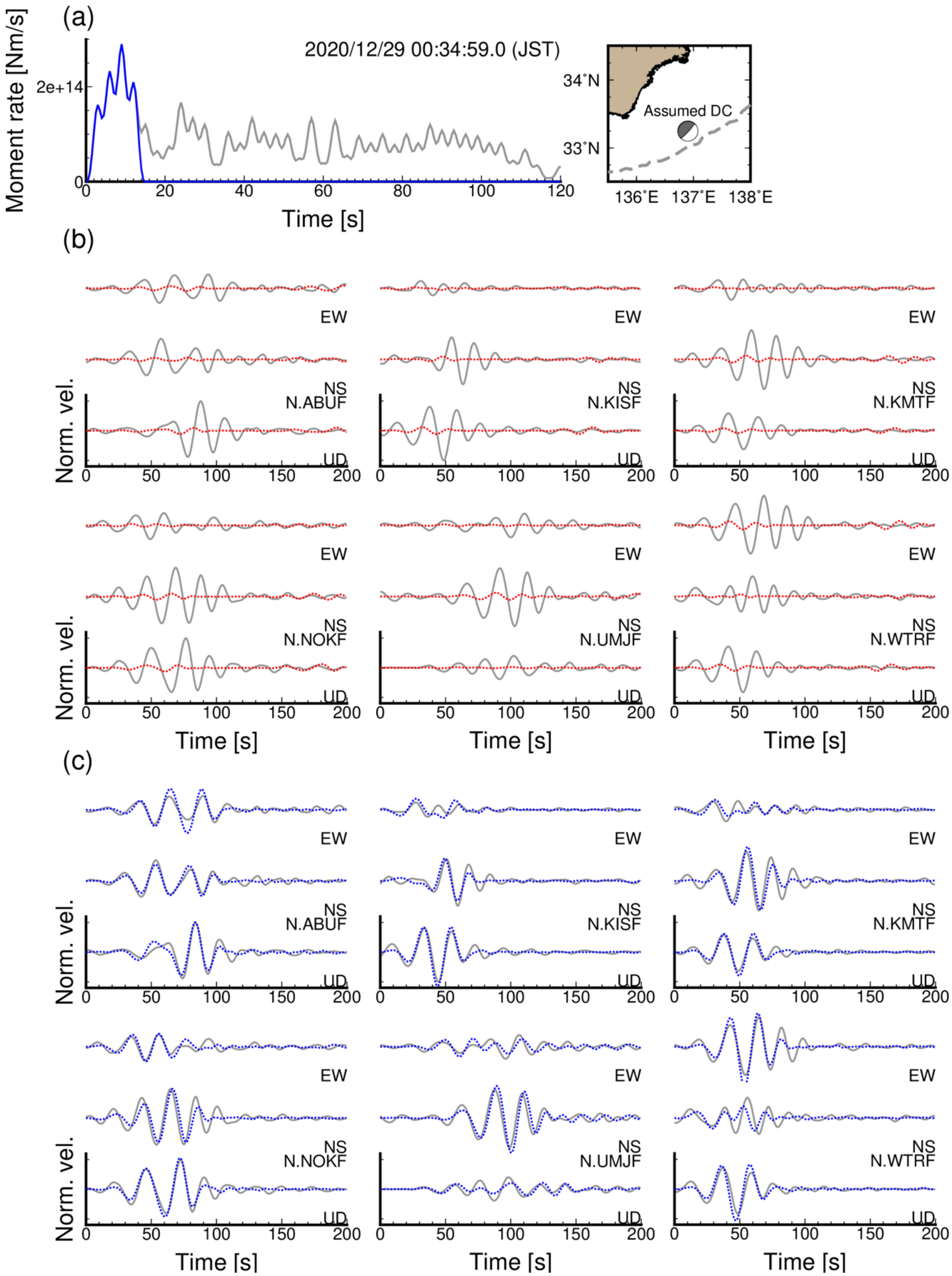

Figure S3. Same as Figure 2 but for adapted parameters, i.e., those representing 85 % of the VR_m between observed and synthetic seismograms.

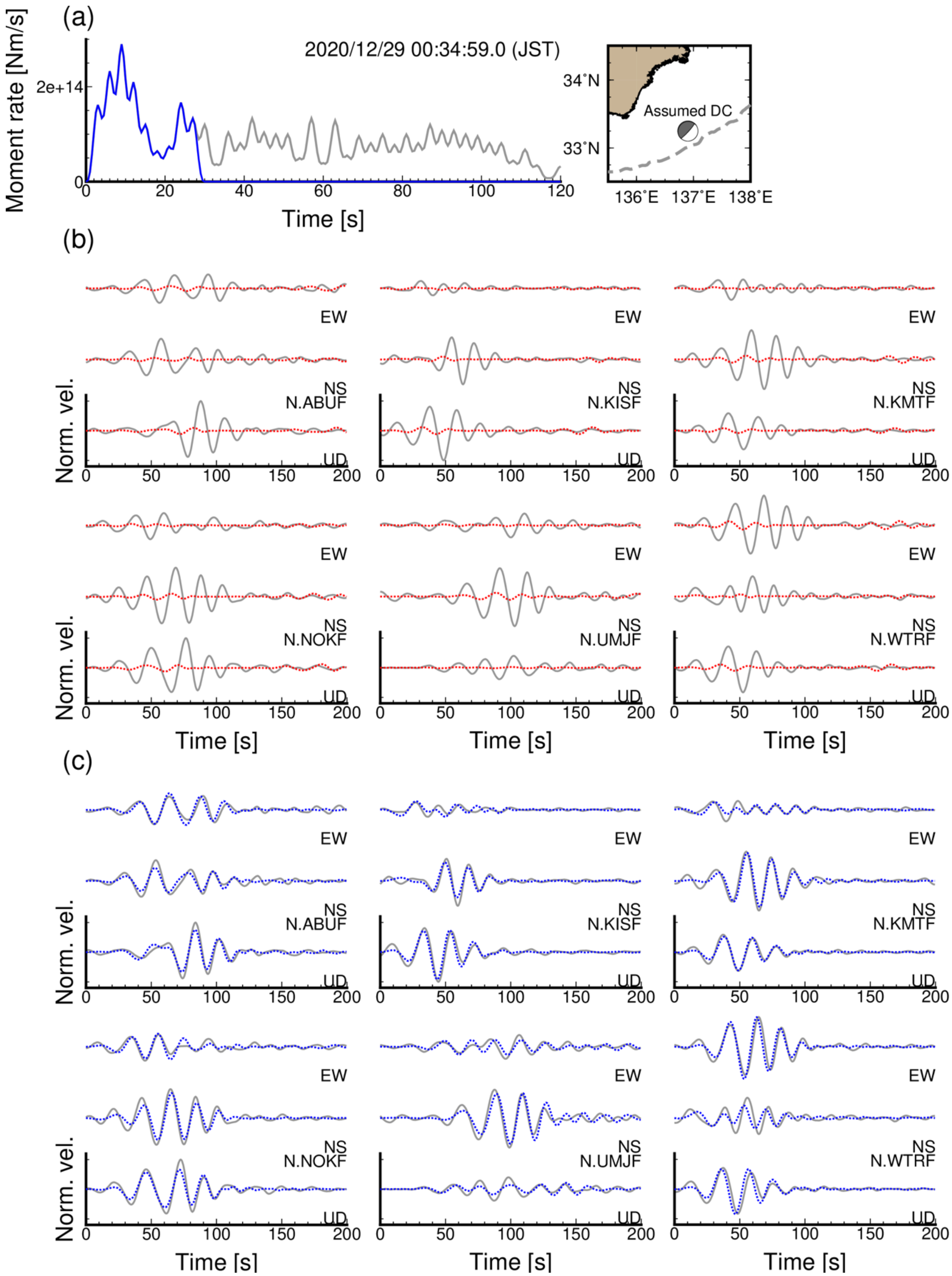

Figure S4. Same as Figure 2 but for adapted parameters, i.e., those representing 95 % of the VR_m between observed and synthetic seismograms.

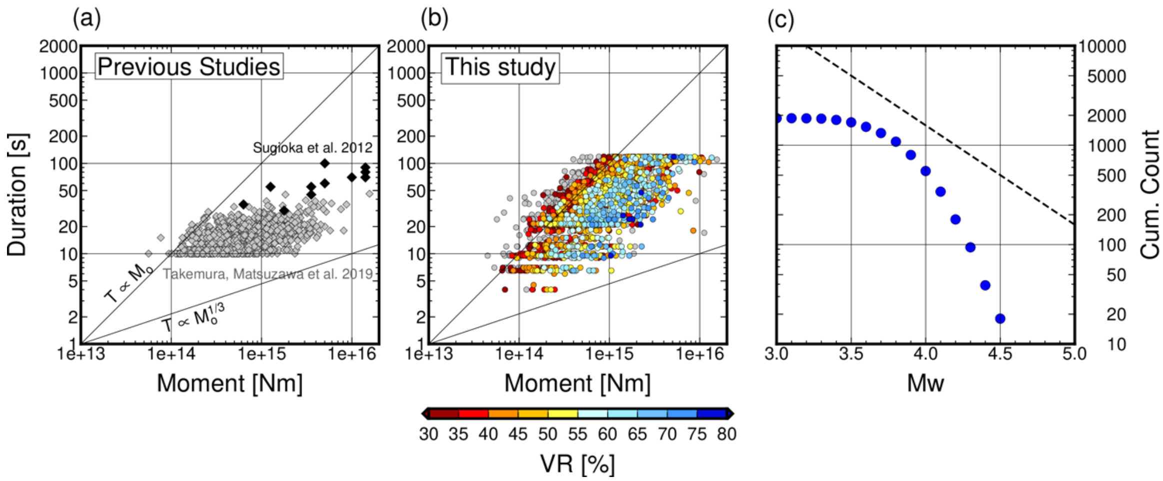

Figure S5. Same as Figure 3 but for adapted parameters, i.e., those representing 85 % of the VR_m between observed and synthetic seismograms.

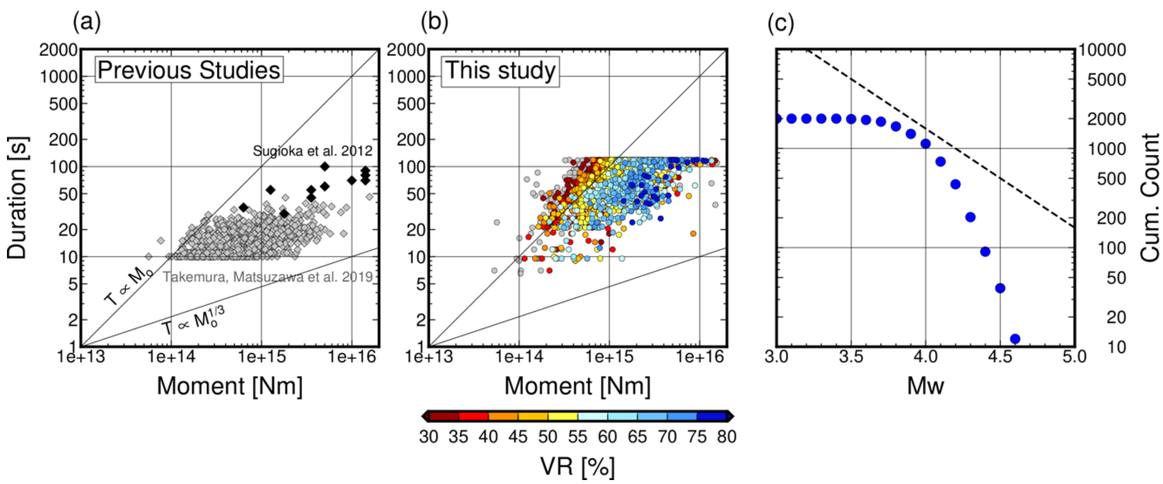

Figure S6. Same as Figure 3 for adapted parameters, i.e., those representing 95 % of the VR_m between observed and synthetic seismograms.

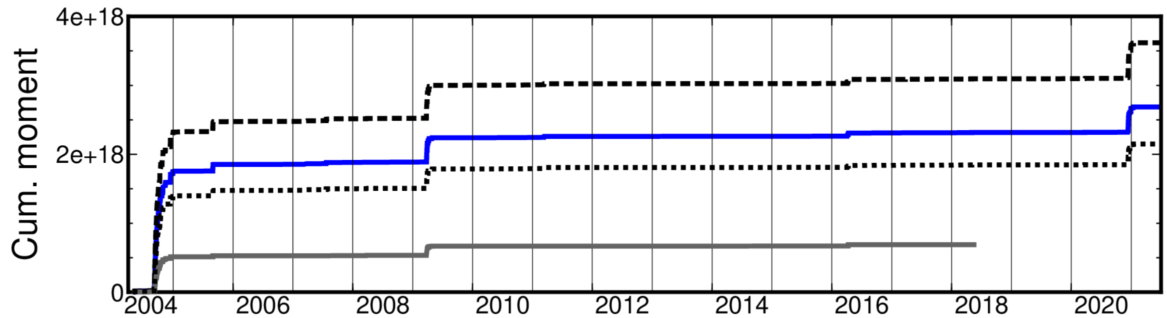

Figure S7. Temporal variations of the cumulative moment of shallow VLFEs southeast of the Kii Peninsula. Blue and gray lines are the same as in Figure 4a. Dashed and dotted lines are derived from the estimated source time functions with adapted parameters, i.e., representing 85 % and 95 % of the VR_m between observed and synthetic seismograms, respectively.

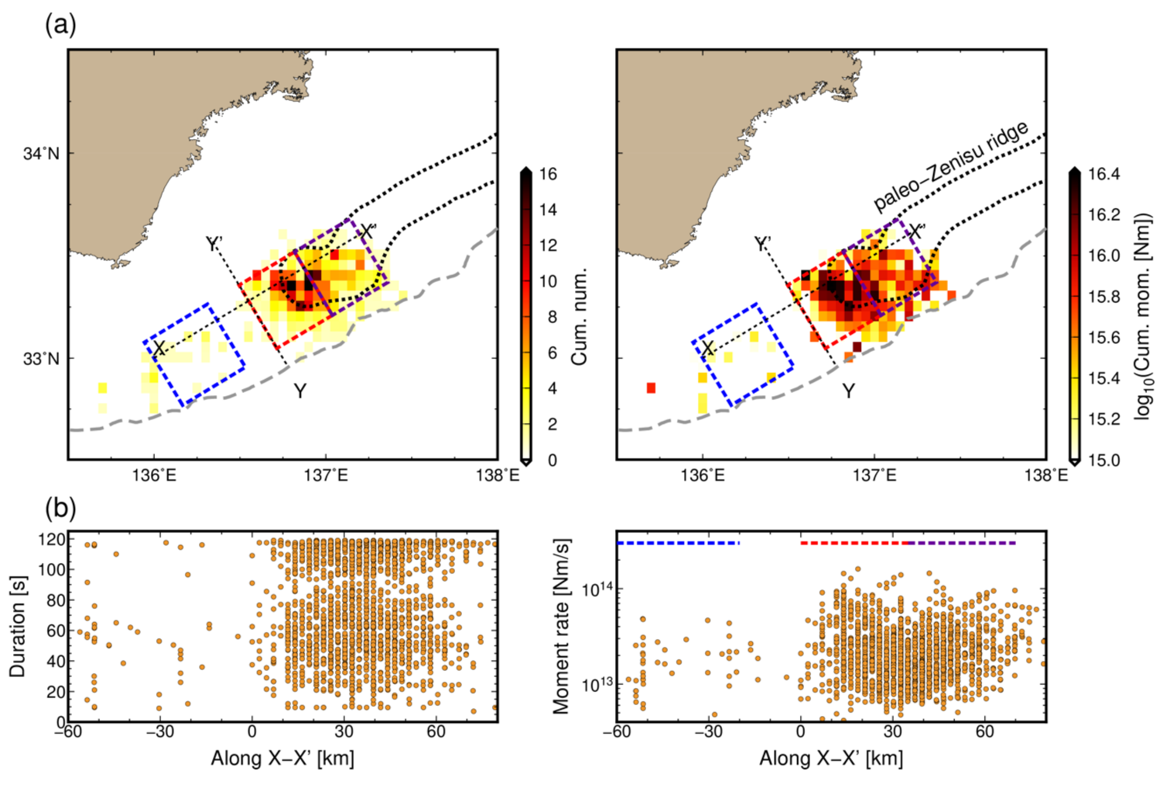

Figure S8. Same as Figure 5 but for adapted parameters, i.e., those representing 95 % of the VR_m between observed and synthetic seismograms.

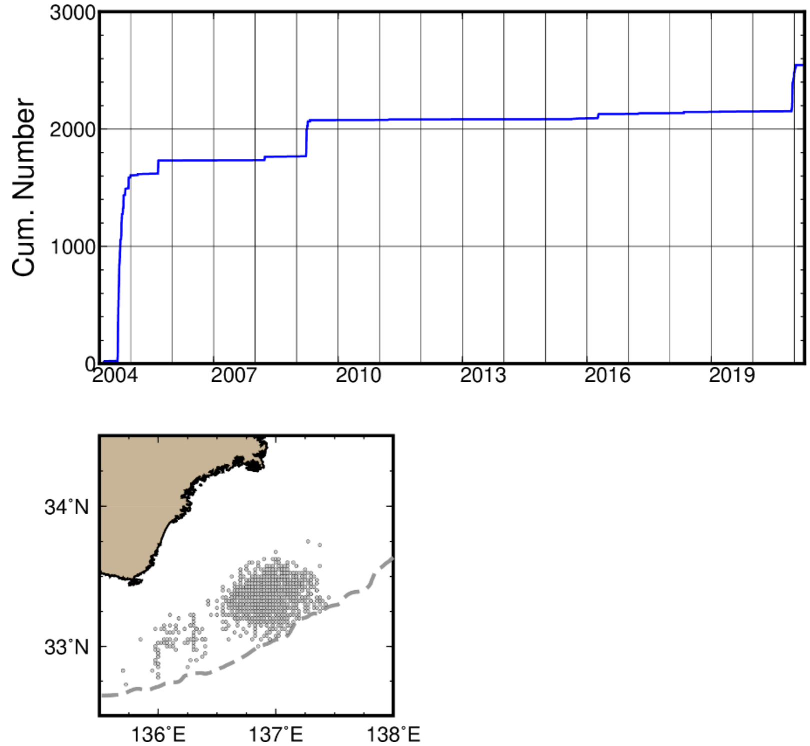

Figure S9. Cumulative numbers of detected shallow VLFEs. Lower map shows the spatial distributions of the detected shallow VLFEs.

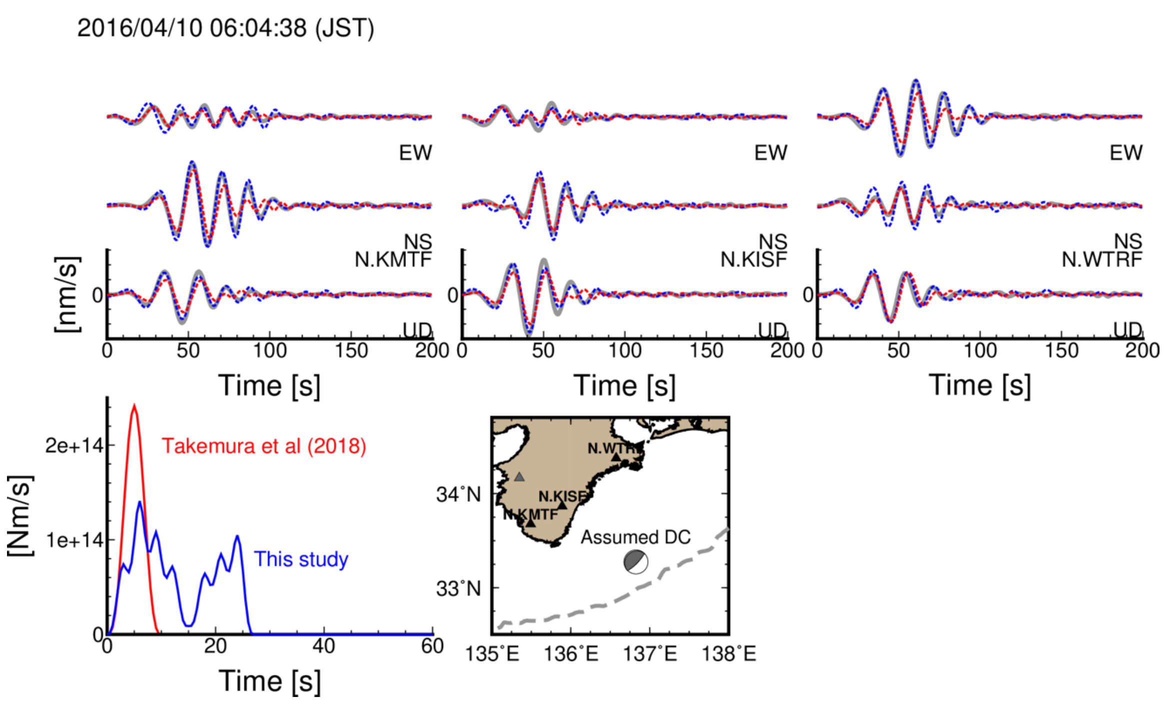

Figure S10. Comparison of estimated moment rate functions between this study (blue lines) and previous study (red lines, Takemura et al. 2018). In upper panel, gray, red, and blue lines represent the observed waveforms, synthetic waveforms of Takemura et al.

(2018), and synthetic waveforms of this study, respectively. A band-pass filter of 0.02–0.05 Hz was applied. Station locations are shown on the map. Estimated moment rate functions are illustrated in the left bottom panel. Estimated seismic moments of Takemura et al. (2018) and this study are 1.02×10^{15} and 1.67×10^{15} Nm, respectively.

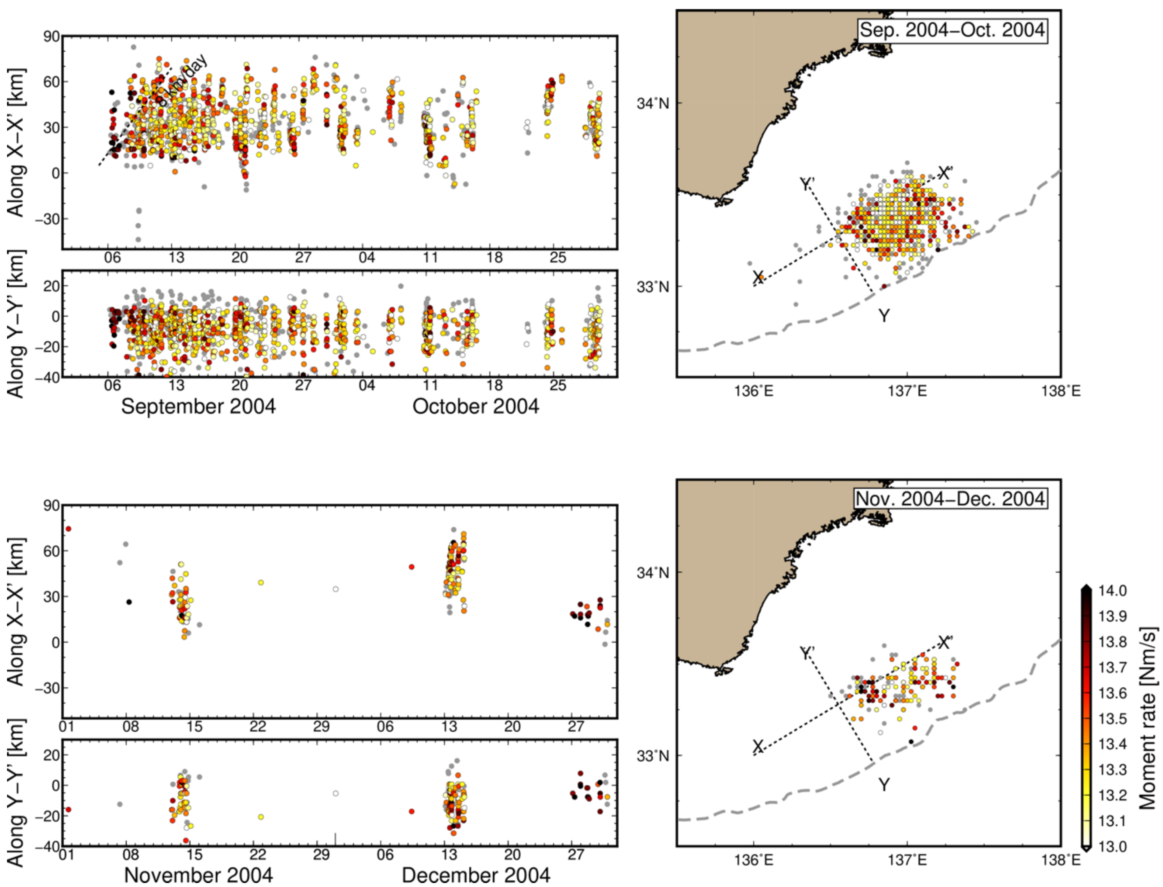

Figure S11. Spatiotemporal variation of a shallow VLFE episode from September 2004 to December 2004. Symbol colors are the same as in Figure 6.

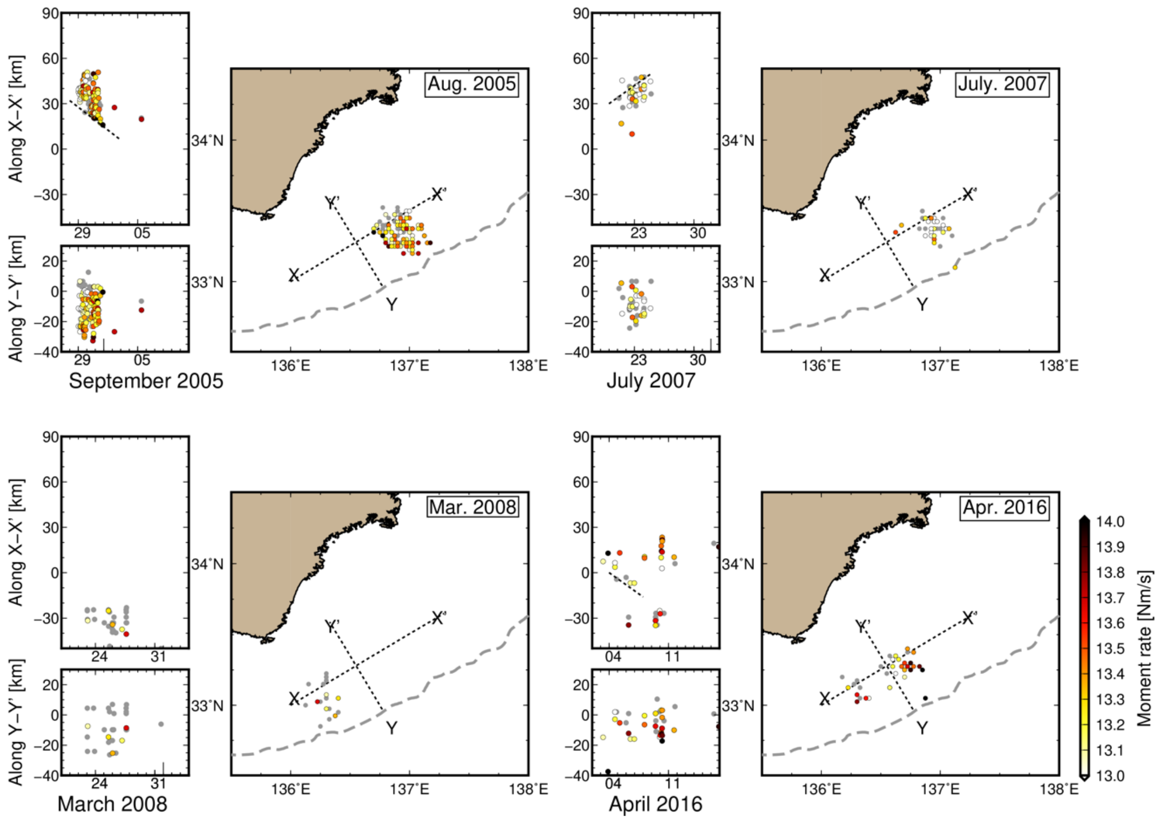

Figure S12. Spatiotemporal variation of shallow VLFE episodes that began in August 2005, July 2007, March 2008, and April 2016. Symbol colors are the same as in Figure 6. Dotted lines represent a migration velocity of 4 km/day.